

# Visualization and Fundamental Analysis of Liquid Atomization by Fuel Slingers in Small Gas Turbine Engines

Werner J.A. Dahm<sup>1</sup>, Prashant R. Patel<sup>2</sup> and Bryan H. Lerg<sup>2</sup>

*Laboratory for Turbulence & Combustion (LTC)  
Department of Aerospace Engineering  
The University of Michigan  
Ann Arbor, MI 48109-2140*

There are strong engineering motivations for wanting to place the design of fuel slingers and the understanding of their performance on an improved technical foundation. To date, however, there have been no studies conducted at a fundamental level of the basic physical processes involved in fuel slinger operation, or of the design and performance rules that are implied by these. We present results from visualization experiments of liquid atomization in a variety of fuel slinger geometries over a range of operating conditions. These visualizations then lead to a fundamental technical analysis that develops broadly applicable design and performance rules for round-hole fuel slingers in small gas turbines. The results from this analysis provide excellent correlation of experimental data by Morishita (1981) on the atomization performance of gas turbine slingers for various combinations of slinger diameters, number of holes, hole sizes, liquid flow rates, and slinger rotation rates. The results provide a basis for understanding the performance of existing fuel slingers, for guiding the design of improved fuel slingers, and for pointing to potentially dramatic new improvements in fuel slinger technology for small gas turbines.

## 1. Introduction

In large gas turbine engines, the liquid fuel burned in the combustor is typically pressure-atomized with a high-pressure fuel pump. However as the dimensions of the engine are reduced, the high-pressure fuel pump does not scale in size or weight with the rest of the engine. As a consequence, in small gas turbines of the type used in business jets, cruise missiles, unmanned aerial vehicles, smart miniature munition systems and various other small turbine engine applications, pressure atomization becomes increasingly disadvantageous. At the same time, the comparatively higher rotation rates at which such small turbine engines can operate, often approaching 100,000 rpm, allow rotary centrifugal atomizers to be used to provide the fuel spray, replacing the high-pressure fuel pump and providing a simple, low-cost, lightweight, and effective means to accomplish the liquid fuel atomization needed for the combustion process. Various types of rotary atomizers are widely used in many different spray processes (*e.g.*, Lefebvre 1989; Bayvel & Orzechowski 1993); the type used in turbine engines is most often referred to as a "fuel slinger". Such fuel slingers have been used for some time in small gas turbine engines (*e.g.*, Rogo & Trauth 1974) and other combustion applications.

To date, the development of such fuel slingers has proceeded on a largely empirical basis. However, since the fuel slinger atomization performance plays an important role in the turbine engine operation, there are strong incentives for wanting to place the de-

sign of such slingers and the understanding of their performance characteristics on an improved technical foundation. Despite this, there have been no openly available fundamental technical studies of the basic design rules and resulting performance correlations that govern fuel slingers. As a consequence, there currently is no fundamentally-rooted technical understanding that exists on which significant improvements in fuel slinger technology can be based. Equally important, there currently is no technical basis from which the operating performance of a fuel slinger in a turbine engine can be reliably inferred from results obtained in simple atomization tests. Similarly, there is no basis on which a fuel slinger that operates successfully in one type of gas turbine engine can be reliably rescaled to another application that involves significantly different size, fuel properties, or operating conditions.

At the most elementary level, a fuel slinger is simply a particular type of rotary atomizer. However, previous research on rotary atomizers has been largely tied to specific geometries and devices, and thus is of limited applicability in developing a fundamental understanding of fuel slingers. At the same time, most basic research on liquid atomization processes has been confined to relatively simple canonical configurations such as mixing layers and jets (*e.g.*, Wu, Ruff & Faeth 1991; Lin & Rietz 1998), in which liquid breakup occurs by very different means than in fuel slingers. Direct numerical simulations are able to investigate certain elementary aspects of liquid breakup in comparatively simple configurations (*e.g.*, Unverdi & Tryggvason 1999), but such simulations cannot yet approach the complex breakup processes involved in liquid atomization by fuel slingers. As a consequence, the existing research literature can provide useful guidance on various fundamental processes involved in liquid breakup, but cannot be directly applied to understand or optimize

<sup>1</sup> Professor of Aerospace Engineering. AIAA Associate Fellow. Corresponding author.

<sup>2</sup> Undergraduate Student, Aerospace Engineering. Member AIAA.

Copyright © 2002 by Werner J.A. Dahm.

liquid atomization in fuel slingers.

The present study provides flow visualization results for the liquid breakup process in fuel slingers over a range of hole geometries, hole sizes, and slinger rotation rates. These visualizations are then used to identify the basic physical processes relevant to liquid atomization with fuel slingers. Analyses of these elementary physical processes are then used to develop fundamental design rules and performance correlations for the liquid atomization properties of fuel slingers under conditions applicable to practical operation of small gas turbine engines. The resulting fundamental performance correlations are then applied to available data on the atomization performance of gas turbine fuel slingers for various combinations of slinger diameters, number of holes, hole sizes, liquid flow rates, and slinger rotation rates. The results provide strong support for the performance correlations obtained in this study, and provide a rational technical basis on which fuel slinger technology can be improved.

## 2. Fuel Slinger Design and Operating Parameters

Figure 1 shows a generic representation of the key aspects of a fuel slinger. The axisymmetric slinger disc rotates at a rate around its centerline. There are a total of  $N$  identical and equally spaced channels located in the slinger rim and oriented along the radial direction. These channels are typically holes with diameter  $d$  or slots with minimum dimension  $d$ , but in principle could be any shape that produces desirable atomization performance. The entrance to each channel is located at radius  $R_1$  from the disc centerline, and the exit at radius  $R_2$ ; the channel length is thus  $(R_2 - R_1)$ . Fundamental considerations in §4 indicate that, for a given hole shape, the parameters associated with the slinger geometry and hole characteristics primarily affect the liquid film thickness  $t$  in the slinger channels. The atomization performance thus involves as relevant parameters the film thickness  $t$ , the slinger channel diameter  $d$ , and the crossflow velocity  $U_c = R$

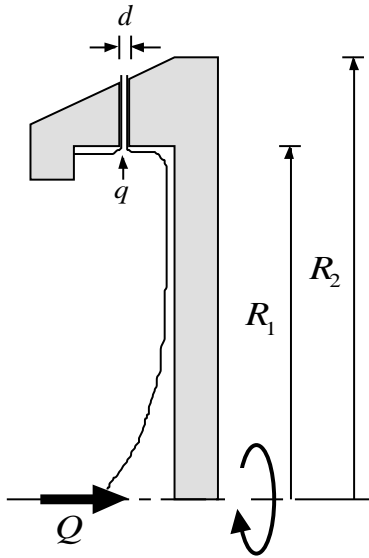


**Fig. 1.** Identification of relevant geometric parameters describing a generic fuel slinger. The rotation rate around the centerline is  $\Omega$ . The slinger rim has inner radius  $R_1$  and outer radius  $R_2$ . Liquid flows across slinger hub and rim, and into channels. The total liquid flow rate is  $Q$ ; the flow rate per channel is  $q$ .

into which the film issues at the channel exit, together with the liquid and gas properties.

### 2.1 Round-Hole Slingers

Any aspect of slinger atomization performance (*e.g.*, mean drop size, drop size dispersion, drop trajectories, etc.) would thus be expected to depend on the following physical parameters:

Liquid film thickness	:	$t$	[L]
Channel diameter	:	$d$	[L]
		hole shape	[--]
Gas crossflow velocity	:	$U_c$	[L/T]
Liquid properties	:	$\rho_L$	[M/L <sup>3</sup> ]
		$\mu_L$	[MLT <sup>-1</sup> ]
		$\sigma$	[M/T <sup>2</sup> ]
Gas properties	:	$\rho_G$	[M/L <sup>3</sup> ]
		$\mu_G$	[MLT <sup>-1</sup> ]

From these 8 relevant parameters involving 3 fundamental units [M, L, T], there are 5 dimensionless parameters that can be formed. The particular choice of these five parameters is irrelevant, since any one set of choices can always be expressed as an algebraic combination of any other set of choices. Thus nondimensional drop sizes, drop size dispersion, drop trajectories, and other aspects of the slinger atomization performance should depend solely of the following five nondimensional parameters:

$$\text{Relative film thickness } s : [t/d] \quad (2.1a)$$

$$\text{Weber number } We : \frac{\rho_G U_c t}{\sigma} \quad (2.1b)$$

$$\text{Ohnesorge number } Oh : \frac{\mu_L}{(\rho_L \sigma t)^{1/2}} \quad (2.1c)$$

$$\text{Liquid-gas density ratio } r : [\rho_L/\rho_G] \quad (2.1d)$$

$$\text{Liquid-gas viscosity ratio } m : [\mu_L/\mu_G] \quad (2.1e)$$

The Weber number  $We$  as defined here gives the ratio of the dynamic forces that the gas exerts on the liquid to the surface tension forces that act on liquid surface. Similarly, the Ohnesorge number  $Oh$  gives the ratio of the viscous forces within the liquid to the surface tension forces that act on the liquid. Together these two parameters express the relative importance of the three key physical effects involved in the atomization process: inertia, viscous diffusion, and surface tension.

### 2.2 Arbitrary Hole Geometries

For slingers with noncircular holes, in addition to the dimensionless parameters in §2.1, the hole shape will also affect the liquid breakup process. It will be seen in the flow visualization results in §3, however, that for the holes geometries considered here, the principal effect of the hole shape appears to be via the transition from “subcritical” to “supercritical” liquid breakup.

For the two circular holes in Table 1, the radius of curvature is everywhere the same, and thus surface tension is pulling the film together with equal tension along the entire periphery of the hole. The film will thus maintain a roughly uniform thickness

over the entire periphery of the hole. Once the resulting film issues from the edge of the hole, the surface tension will act to collapse the film together toward its center. The time scale on which this collapse occurs can be obtained from simple scaling considerations as

$$\sim \frac{d^2 t}{L} \quad (2.2)$$

If this time scale is sufficiently small relative to the characteristic bulk time scale with which the film issues from the hole, namely

$$(U_b/d) = \frac{L a t^3}{3 \mu L d} \quad (2.3)$$

where the bulk liquid speed  $U_b$  is given in §4, then surface tension should collapse the film into a single concentrated ligament having a diameter much larger than the original film thickness. On the other hand, if  $L a t^3$  is sufficiently large in comparison with  $(U_b/d)$ , then the film will break up due to inertial forces before surface tension can draw it together. The latter case, termed “supercritical liquid breakup” will produce much finer drops than the “subcritical liquid breakup” in the former.

For noncircular holes, the transition between these two liquid breakup regimes will depend on the hole shape. Some parts of the liquid film will issue from portions of the hole where the local radius of curvature in the hole geometry is sufficiently large that surface tension is unable to pull the film into a single concentrated ligament. These parts of the film thus form many comparatively thinner ligaments. By contrast, where the local radius of curvature of the hole is sufficiently small, surface tension is strong enough relative to the liquid inertia to pull the nominally thin liquid film together into a concentrated ligament. The concentrated ligaments formed in this manner thus have a significantly larger diameter than those formed from instabilities of the liquid film. When these larger ligaments subsequently break up, they form larger diameter drops.

For slot holes of the type in Table 1, it may be anticipated that over the central portion of the slot, where the radius of curvature is infinite, the liquid will issue from the hole as a film and thus will show locally “supercritical breakup”. However at the ends of the slot, where the radius of curvature is small, the liquid will be drawn into relatively large diameter ligaments, and those parts of the film will undergo “subcritical breakup”. For the square holes in Table 1, the extremely small radius of curvature at the four corners would then be expected to draw the liquid film into four concentrated ligaments emanating from these corners.

Once the problem has been formulated in these terms, it becomes essentially a generic liquid stream atomization problem, and differs from other such problems only in the initial geometry of the liquid as it exits from the channel. This allows the large body of basic research literature that exists on the subject of liquid atomization in round jets and other configurations to be properly applied to fuel slingers to obtain quantitative insights into their resulting atomization performance. Specifically, as will be seen in §§4.3 and 4.4, prior research has shown that primary breakup of liquid streams and any subsequent secondary breakup of the resulting drops occurs by just a few specific mechanisms that are determined by the values of  $We$ ,  $Oh$ ,  $r$ , and  $m$ . By using these prior results, it is possible to dramatically reduce the number of tests required for a comprehensive performance characterization,

and focus largely on the effects of the relative film thickness  $s$  that distinguishes fuel slinger atomization from atomization in round jets and other configurations.






### 3. Visualizations of Liquid Breakup in Fuel Slingers

Instantaneous visualizations of the liquid break process for various slinger hole geometries over a range of rotation rates were obtained using Nd:YAG laser-based flash photography. The results from these visualizations provide the basis for the analyses of slinger atomization performance given in §4 and §5.

#### 3.1 Experimental Arrangement

Five different slinger geometries were considered, as shown in Table 1. Each slinger consisted of a 4-in. diameter disc with a rim containing 16 identical equally-spaced slinger holes. The disc diameter is representative of typical values for slingers used in small gas turbine engines. The slinger rim was flat on both sides, with an inner diameter of 3.75-in. and an outer diameter of 4.00-in. Slinger holes in the desired shape were EDM fabricated with very fine tolerance straight through this rim, producing 0.125-in. long channels through which the liquid flowed from the disc to issue from each of the slinger holes. The hole sizes in Table 1 were chosen so that the large round (LR) and short slot (SS) holes produced the same “equivalent diameter”  $d$  (see §4.1.4) to allow a test of this equivalence concept.

The slinger axis was connected via a shaft and chuck to a router motor, the speed of which could be set by an electronic controller. The router speed at each controller setting was measured using a strobe light. Slinger rotation rates were held constant ( $\pm 100$  rpm drift in the router motor speed) at speeds ranging from 900 - 17,800 rpm. These rotation rates span the representative range of engine relight conditions in small gas turbine engines. Tap water was fed onto the center of the rotating slinger disc via a pump, with the total liquid flow rate supplied to the slinger being controlled and measured by an in-line rotameter. For all cases considered in the present experiments, the liquid flow rate was kept constant at 8 gpm, which is representative of practical fuel flow rates in small gas turbines at these speeds.

Hole Shape	Dimensions	
Small Round	0.75 mm	
Large Round	1.5 mm	
Square	1.5 mm × 1.5 mm	
Short Slot	0.5 mm × 2 mm	
Long Slot	0.5 mm × 4.5 mm	

**Table 1.** Hole shapes and dimensions for the five slingers, denoted SR, LR, SQ, SS and LS, used in the liquid breakup visualization experiments. The LR and SS holes have the same equivalent diameter  $d$  (see §4).

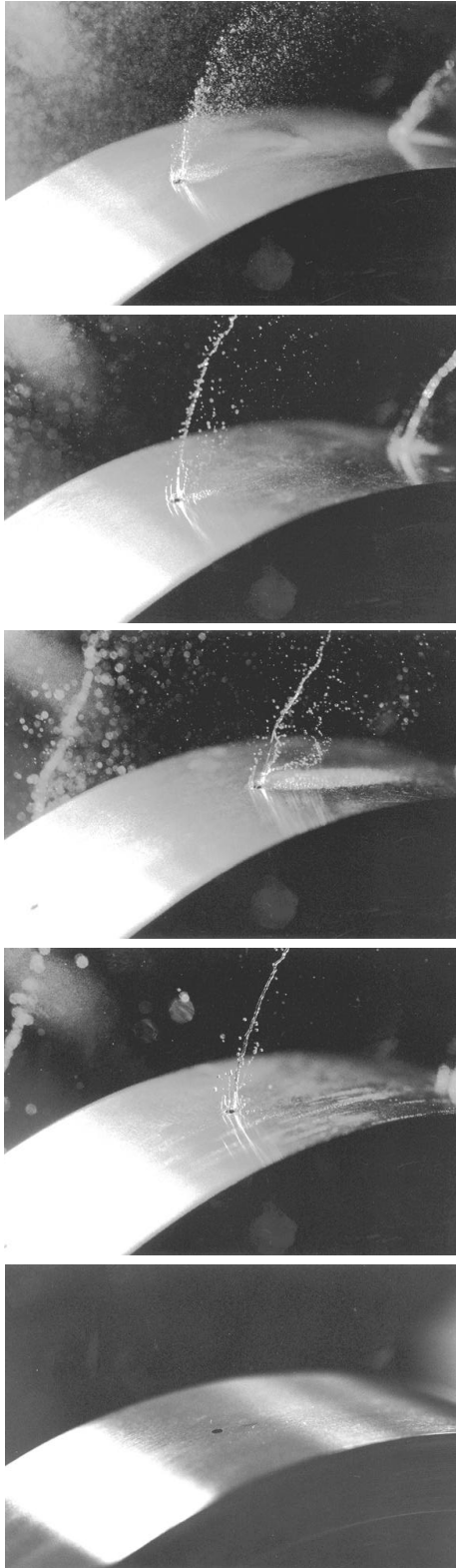


**Fig. 2.** Typical visualizations of the liquid breakup process for small round hole (SR) slingers, showing hole geometry (*bottom*) and atomization performance at rotation rates of 4300 rpm, 7800 rpm, 9500 rpm and 17,800 rpm (*top*).

The liquid issued from the slinger holes into room air at nominally 30 °C and 1 atm. Only the slinger rotation rate and the hole geometry were varied.

Visualizations were obtained by indirectly illuminating the liquid breakup process with 532 nm light pulses of 10 nsec duration from a frequency-doubled Nd:YAG laser. A simple 35 mm camera recorded the breakup pattern on standard ISO 100 film using a Vivatar macro lens. The camera was positioned to provide both oblique and side views of the liquid breakup process. For the side view experiments, a ground glass screen placed behind the slinger provided for diffuse backlit illumination, with the screen placed well out of focus to eliminate laser speckle. The typical field of view was roughly 2-in  $\times$  1.25-in.; the practical depth of field was about 0.5-in. The resulting photographs were subsequently scanned at relatively high resolution to provide enlarged views of the liquid breakup process. No image processing was performed other than simple brightness and contrast adjustment. For any given hole geometry at any fixed rotation rate, the liquid breakup pattern was observed to be highly repeatable, despite the fact that strikingly different features were seen in the breakup patterns at different rotation rates and for different hole geometries.

### 3.2 Visualization Results

Figures 2-6 show oblique views of the liquid breakup process for each of the five slinger hole geometries at rotation rates of 4300, 7800, 9500, and 17,800 rpm. The dimensionless liquid-gas density and viscosity ratios are the same in all these cases, and thus effects of  $r$  and  $m$  cannot be investigated here, but the results suggest clear trends in the breakup patterns and drop sizes as  $We$  increases with increasing rotation rate. In general, as would be expected, the drop sizes become smaller with increasing  $We$ . Significant differences are also seen in the breakup patterns at the same rotation rate among the various hole geometries examined in these figures. The effect of  $Oh$  is less apparent, since this changes solely via the nominal film thickness  $t$ , which varies with rotation rate, hole size, and hole geometry (see §4). Ohnesorge number effects will be addressed in §4.

Figures 7-15 compare enlarged views of certain key phenomena that appear to be of central importance in these liquid breakup processes. Figure 7 shows two representative oblique views of liquid breakup from the large round (LR) slinger holes at very low rotation rate, corresponding to low values of  $We$ . There are two features of particular importance that are evident in the resulting pattern. First, it is apparent that at these conditions the liquid film issues from the *entire* periphery of the hole. The side views in Fig. 8 verify that this is indeed the case. Coriolis effects at this low rotation rate are apparently not sufficiently strong to accumulate liquid on the side of the hole opposite to the direction of rotation. The relatively short channel lengths in these slingers may also be important in avoiding such liquid accumulation due to Coriolis effects. Evidence will be seen below, at higher rotation rates, that for the present slingers this appears to remain the case at all the rotation rates examined here. Conditions under which such liquid accumulation should occur are examined in §4.

Second, it is apparent in Figs. 7 and 8 that these conditions correspond to “subcritical liquid breakup”, in which surface tension causes the hollow liquid film issuing from the periphery of the

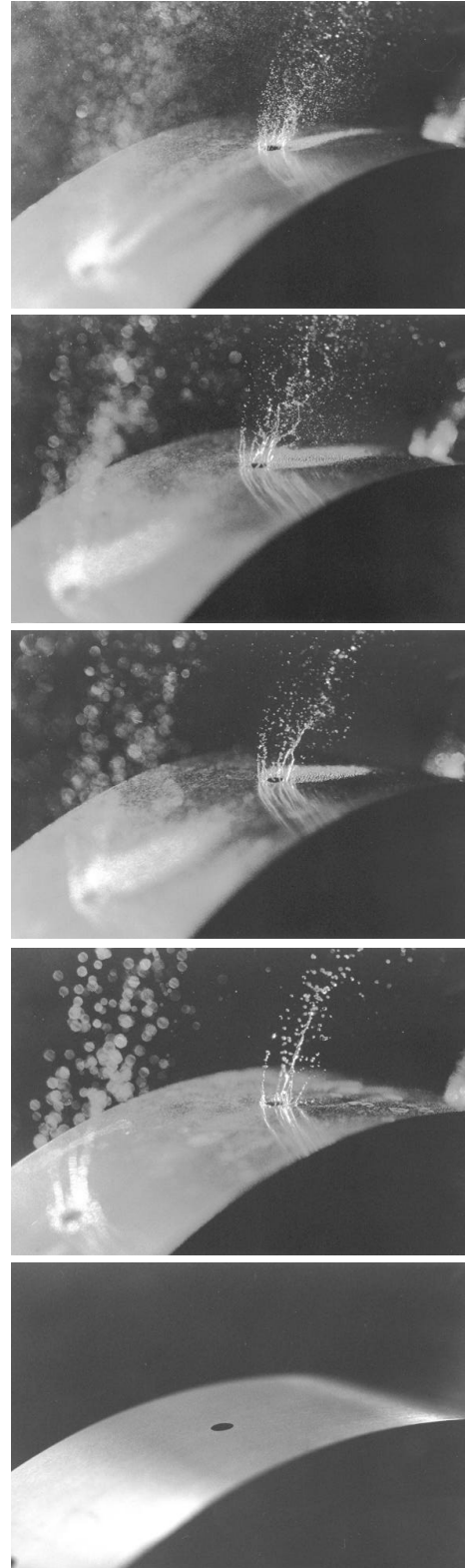
hole to be drawn together as it leaves the slinger, and thereby to collapse into a single liquid ligament. As noted in §2, such subcritical breakup should occur when the time scale for collapse of the liquid film is sufficiently short in comparison with the inertial time ( $U_b/d$ ). In subcritical breakup, the ligament formed from the initially thin liquid film has a diameter much larger than the initial film thickness  $t$ . Once this large ligament is formed from the film, it appears to break up by the classical Rayleigh mechanism, enhanced by the relatively large disturbances introduced in the liquid as the film collapses due to surface tension. As a consequence, the resulting drop sizes are comparable to the ligament diameter.

Figure 9 compares subcritical breakup in the large round (LR) and short slot (SS) slingers at otherwise identical conditions. Recall that these two cases have essentially the same “equivalent diameter”  $d$  (see §4.1.4). Note that in both cases the liquid film initially issues from the entire periphery of both holes, but is then rapidly drawn together by surface tension into a large ligament; this subsequently undergoes Rayleigh breakup to form relatively large drops. Since the diameters of the resulting ligaments in both cases are comparable, the drop size distribution should also be similar, and this appears to be the case. As a consequence, in subcritical breakup the hole geometry appears to have at most a weak effect on the liquid breakup process and the resulting drop size distribution.

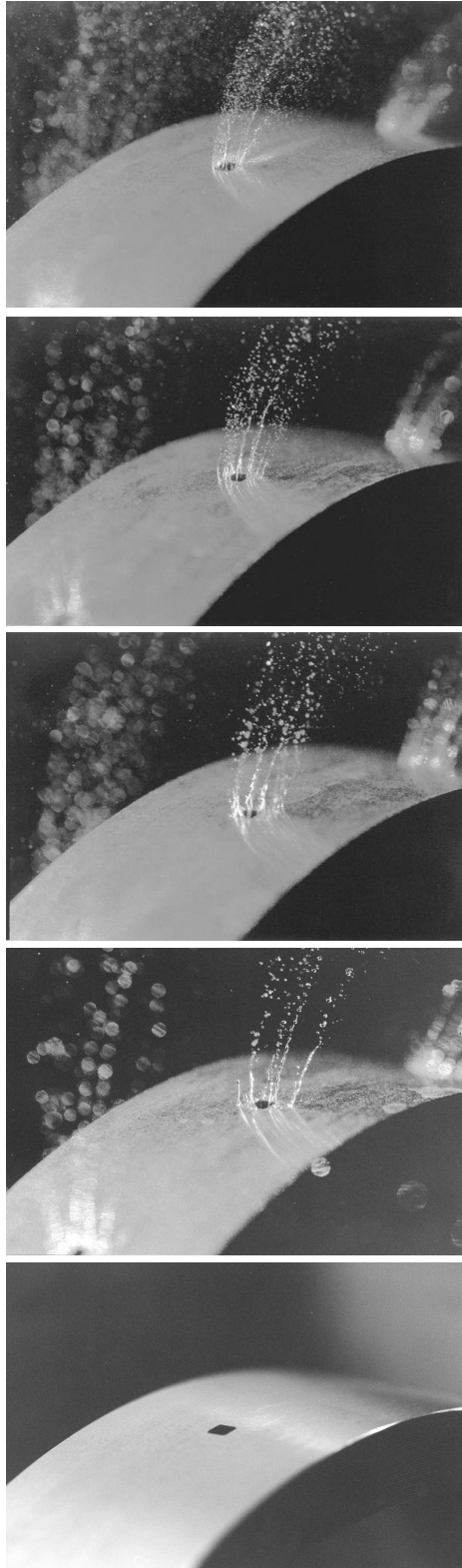
Figure 10 compares “subcritical” and “supercritical” liquid breakup in the short slot (SS) slinger. As noted in §2, the latter corresponds to conditions for which the time scale in (2.2) required for collapse of the liquid film is not fast enough in comparison with the inertial time ( $U_b/d$ ) in (2.3). As a result, inertial effects act to tear the liquid film issuing from the hole into smaller ligaments before surface tension can act to pull the film together into a single large ligament. These resulting smaller ligaments then appear to undergo classical Rayleigh breakup into drops with diameters roughly comparable to the ligament diameters. For the relatively low rotation rate in Fig. 10*b*, the liquid sheet forms into just a few ligaments, which therefore have diameters only somewhat smaller than the single large ligament in Fig. 10*a*.

Figure 11 shows a similar comparison of subcritical and supercritical liquid breakup for the square hole (SQ) slinger. For the subcritical case in Fig. 11*a*, the diameter of the resulting single ligament is comparable to those in Figs. 7-9 and 10*a*. For the supercritical breakup in Fig. 11*b*, the liquid again initially issues in a thin film from the entire periphery of the hole, but now the very high surface tension in the four corners of the square film, where the radius of curvature is exceedingly small, acts to pull the film into four more or less distinct ligaments. It is possible that some concentration of the liquid in these corners occurs even as the liquid film flows along the channel walls before issuing from the hole, however the fact that the film is constrained directly at the wall suggests that this effect may depend strongly on the film thickness (see §4.1). The resulting ligaments again appear to undergo a classical Rayleigh breakup to form drop sizes comparable to the resulting ligament diameters.

Figure 12 shows another phenomenon found at relatively low rotation rates for several of the hole geometries in this study. It is apparent in both the examples shown in this figure that the liq-



**Fig. 3.** Typical visualizations of the liquid breakup process for large round hole (LR) slingers, showing hole geometry (*bottom*) and atomization performance at rotation rates of 4300 rpm, 7800 rpm, 9500 rpm and 17,800 rpm (*top*).



**Fig. 4.** Typical visualizations of the liquid breakup process for square hole (SQ) slingers, showing hole geometry (*bottom*) and atomization performance at rotation rates of 4300 rpm, 7800 rpm, 9500 rpm and 17,800 rpm (*top*).

liquid film initially issues from the entire periphery of the hole. However, at these low rotation rates the inertial effects in the liquid are sufficiently small in comparison with the surface tension that, upon issuing from the hole, the liquid film flows *along* the slinger face *away* from the hole, rather than immediately separating from the slinger face at the edge of the hole. The liquid thus accumulates on the slinger face in the vicinity around the hole, while inertia causes the resulting liquid pool to form irregular ligaments, which then undergo subsequent breakup into drops. Owing to the irregular nature of the ligament formation, the variance in the drop size distribution should be much larger than when the film forms into more regular ligaments, as in the previous figures. The tendency of the liquid film to flow away from the hole along the slinger face can be seen in several of the cases in Figs. 2-6, but the effect appears most pronounced for the square hole (SQ) slinger; this may be connected with the higher surface tension in the four corners of the SQ slinger.

Figure 13 shows two representative examples of the liquid breakup process on the square hole (SQ) slinger at a somewhat higher rotation rate than in Fig. 12. Under these conditions, the film only spreads along the slinger face for a small distance away from the hole, and as a result the liquid breaks up into a much more regular pattern of ligaments, and thus a more nearly monodisperse distribution of drops.

Figure 14 shows the effect of further increases in the rotation rate for the square hole (SQ) slinger. The liquid breakup patterns seen at these two higher rotation rates should be compared with those at intermediate rotation rate in Fig. 13, and at very low rotation rate in Fig. 12. It is apparent in Fig. 14a that the liquid film still flows away from the square hole, but it now breaks up into a larger number of ligaments having correspondingly smaller diameters. These ligaments in turn break up into finer droplets, presumably via the Rayleigh mechanism. In Fig. 14b, at very high rotation rate, this progression continues with the film rapidly breaking up into many smaller ligaments and smaller drop sizes (see also Fig. 4).

A similar progression is evident in Fig. 15 for the long slot (LS) slinger (see also Fig. 6). At the very low rotation rate in Fig. 15a, the comparatively large effect of surface tension near the ends of the slot, where the radius of curvature is small, concentrates the liquid film there to produce relatively large diameter ligaments originating from the ends of the slot. This is a manifestation of locally subcritical breakup from a noncircular hole geometry. Over the central portion of the slot, where the film has no curvature, surface tension does not act and the film instead flows along the slinger face away from the hole, until it eventually breaks up into ligaments. At the very high rotation rate in Fig. 15b, corresponding to supercritical breakup, careful inspection reveals that the liquid film still initially flows along the slinger face upon exiting from the hole, but breaks away from the slinger face much closer to the hole into much smaller ligaments to produce much finer drops.

Collectively, these visualization results show that, for the hole geometries considered here, there appear to be just a few relatively distinct phenomena involved in the liquid breakup process. The relative importance of each of these phenomena changes as the hole shape, the hole size, or the slinger rotation rate is varied. However all of these phenomena appear to result

primarily from various competing effects of inertia and surface tension, and they should thus principally correlate with the Weber number  $We$ . In the following section, simple analyses of various physical processes relevant to the film formation and breakup will be considered, which then lead in §5 to the proper variables in which performance correlations can be written for liquid atomization by fuel slingers under conditions applicable to small gas turbine engines.

#### 4. Fundamental Physical Processes in Fuel Slingers

Basic physical considerations reveal that there are four key sequential processes relevant to the liquid atomization performance of fuel slingers: (i) liquid film formation, (ii) film instabilities and other nonuniformities, (iii) primary liquid breakup, and (iv) secondary breakup of drops. This section considers each of these processes individually, and develops design rules for each that then provide the basis for the resulting overall performance correlations for fuel slingers in §5.

##### 4.1 Fuel Slinger Film Thickness

The liquid film thickness produced by a fuel slinger is one of the key parameters relevant to its atomization properties. This section analyses the liquid flow within the slinger channels, since this plays a key role in the primary liquid breakup process at the channel exit, which in turn determines the atomization quality.

###### 4.1.1. Liquid film formation

As was indicated in Fig. 1, liquid fuel at density  $\rho_L$  is issued at a total mass flow rate  $M$  onto the slinger hub, corresponding to a total volume flow rate  $Q = M/\rho_L$ . Centripetal acceleration spreads the liquid along the hub and across the inside rim of the slinger. The liquid then flows into each of the  $N$  channels, giving mass flow rate  $m = M/N$  through each channel, with the corresponding volume flow rate on a per-channel basis as  $q = m/\rho_L$ .

When the radius ratio ( $R_2/R_1$ )  $> 1$ , as is typically the case in most practical slingers, then the channel can be considered at a nominal radius  $R = 1/2(R_1 + R_2)$  from the centerline. Liquid fuel in the channel thus experiences centripetal acceleration  $a = R\omega^2$  along the channel. The resulting centrifugal force induced on the liquid in the channel is thus  $\rho_L R\omega^2$ , pointing along the channel, where  $\rho_L$  is the liquid density. As the liquid flows at a characteristic speed  $U$  along the channel, its radial location  $r$  increases and thus its tangential velocity  $r\omega$  also increases. In the reference frame of the channel, this induces a Coriolis (lateral) force  $\rho_L U r\omega$  pointing opposite to the direction of rotation. The relative magnitude of the centrifugal force to this Coriolis force is thus  $R\omega/U = Ro$ , where  $Ro$  is the Rossby number and determines the relative importance of Coriolis effects. Coriolis forces on the flow in the channel will be small when  $Ro \gg 1$ .

It will be seen in §4.1.3 that, for the channels in a “typical” slinger with radius  $R = 5$  cm and  $\omega = 3000$  rad/sec, the peak liquid speed is  $U_p = 11$  m/s and the bulk average liquid speed is  $U_b = 7.5$  m/s. These give a Rossby number of  $Ro = 20$  based on the bulk velocity, indicating that the lateral Coriolis force is typically about 5% of the centrifugal force. The effects of this comparatively small Coriolis force will be addressed in §4.2.4.

Since the liquid wets the entire surface on the inside rim of the slinger, and is subjected to a radially outward (centrifugal) force,

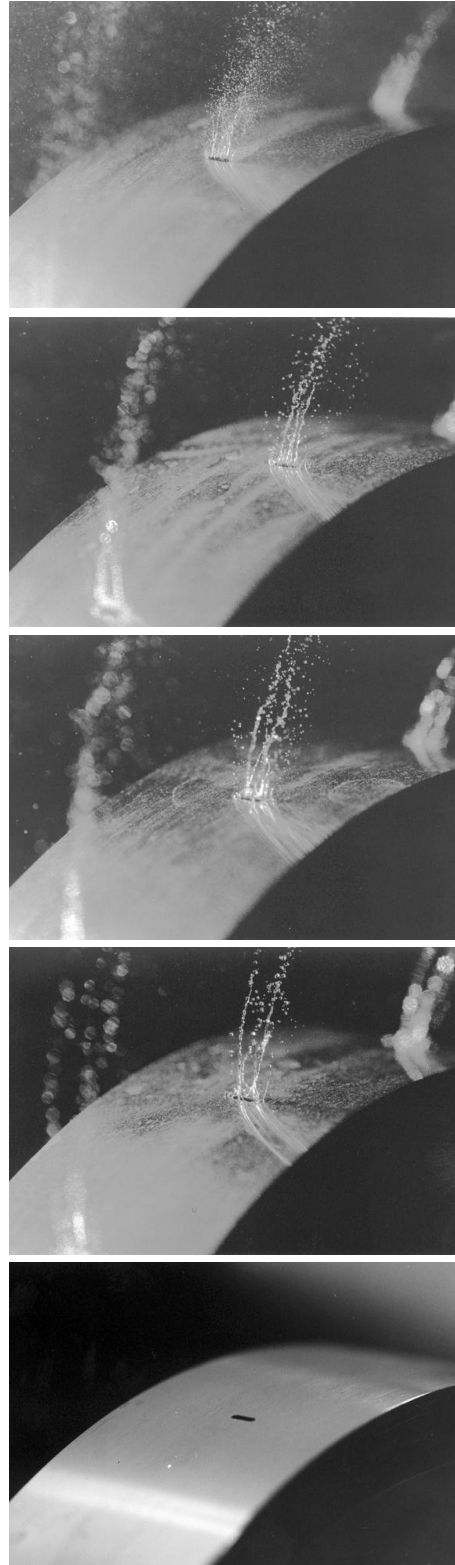


**Fig. 5.** Typical visualizations of the liquid breakup process for short slot (SS) slingers, showing hole geometry (*bottom*) and atomization performance at rotation rates of 4300 rpm, 7800 rpm, 9500 rpm and 17,800 rpm (*top*).

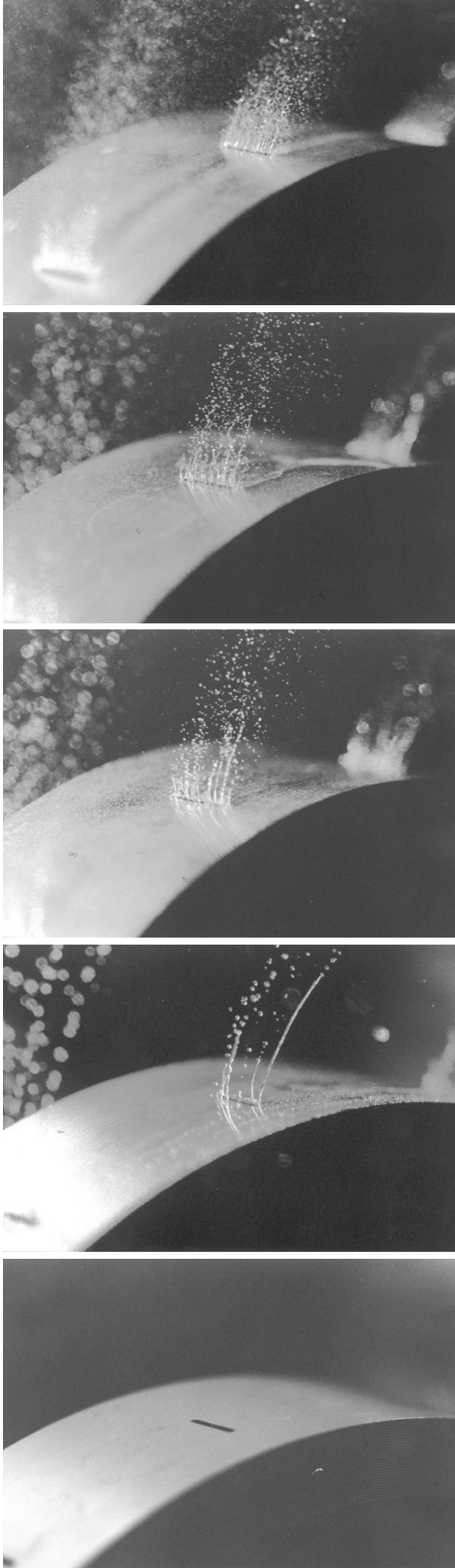


**Fig. 6.** Typical visualizations of the liquid breakup process for long slot (LS) slingers, showing hole geometry (bottom) and atomization performance at rotation rates of 4300 rpm, 7800 rpm, 9500 rpm and 17,800 rpm (top).

it enters along the entire periphery of the channel and thus wets the entire inside surface of the channel. Figure 16 shows the resulting nominal liquid film development within the channel. The initially thick liquid film at the channel entrance is rapidly thinned as the liquid moves under the radial acceleration  $a$ . After a distance  $l$ , the film reaches a constant limiting thickness  $t$  at which the radial outward force due to the centripetal acceleration  $a$  is balanced by the wall shear stress  $\tau_w$  due to the viscous no-slip condition at the channel wall.

From these considerations, it is apparent that channel lengths  $L$  significantly longer than the entrance length  $l$  serve no useful purpose as far as the liquid film thickness is concerned. Once the film is formed on the channel walls, further residence time of the film in the channels serves only to allow surface tension to draw the film into those parts of the cross section with higher curvature, leading to larger ligaments diameters and thus poorer atomization performance. The weight of the slinger can therefore be reduced by keeping the outer radius  $R_2$  fixed, since this determines the centripetal acceleration  $a$ , and increasing the inner radius  $R_1$  so that the resulting channel length  $L = (R_2 - R_1)$  is only slightly longer than the entrance length  $l$ . Furthermore, §4.2.4 shows that there may be very significant advantages in terms of dramatically improved atomization performance by minimizing the channel length  $L$ .

#### 4.1.2. Simple physical model of film thickness

The resulting nominally uniform channel film thickness  $t$  can be obtained from the simple analysis shown in Fig. 17, which also gives certain physical insights into the process. Per unit of channel circumference, the radial outward force induced on the liquid in a control volume of length  $dx$  and thickness  $t$  by the acceleration  $a$  is  $(a_L t dx)$ . The limiting thickness is reached when this is exactly balanced by the radial inward force  $(\tau_w dx)$  due to the wall shear stress, which gives the limiting film thickness  $t$  as  $t = \tau_w / a_L$ . Denoting the characteristic liquid film velocity at the free surface as  $U$ , then the wall shear stress will be  $\tau_w \sim \mu_L (U/t)$ , where  $\mu_L$  is the dynamic viscosity of the liquid fuel. The film velocity  $U$  is then determined by the liquid volume flow rate per unit circumferential distance  $q/d$  and the film thickness  $t$  as  $Ut \sim q/d$ . Recalling that  $a = R^{-2}$  then gives the limiting film thickness as

$$t \sim \frac{\mu_L q}{R^2 d}^{1/3}.$$

This simple analysis serves to identify the physical origin of the limiting film thickness, and shows how it depends on the relevant liquid fuel properties, the slinger design, and operating parameters. Moreover, contrary to what intuition might suggest, smaller channel diameters  $d$  are seen in the result above not to produce a smaller liquid film thickness  $t$ . The analysis instead shows that larger channels will provide for smaller film thickness, since they provide more channel surface area over which the liquid film is spread.

#### 4.1.3. Detailed analysis of liquid film flow

A more complete analysis, which also provides the proportionality constant in the result above as well as the film velocity field, can be obtained from an exact Navier-Stokes solution of the film flow in this limiting state. Referring to Fig. 17, the steady flow in the liquid film is governed by the equations for mass and mo-



momentum conservation, namely

$$\frac{u}{x} + \frac{v}{y} = 0 \quad (4.1a)$$

$$\mu_L \left( u \frac{u}{x} + v \frac{u}{y} \right) = \mu_L \left( -\frac{p}{x} + \mu_L \left( \frac{\partial^2 u}{\partial x^2} + \frac{\partial^2 u}{\partial y^2} \right) \right) \quad (4.1b)$$

$$\mu_L \left( u \frac{v}{x} + v \frac{v}{y} \right) = \mu_L \left( -\frac{p}{y} + \mu_L \left( \frac{\partial^2 v}{\partial x^2} + \frac{\partial^2 v}{\partial y^2} \right) \right) \quad (4.1c)$$

Once the film reaches its limiting thickness, the wall-normal velocity  $v$  is everywhere zero and thus (4.1a) provides that  $u$  will vary in the  $y$ -direction only. From (4.1c) the pressure is then everywhere uniform, and (4.1b) thus gives

$$\mu_L \frac{\partial^2 u}{\partial y^2} = \mu_L a \quad (4.2)$$

which integrates to

$$u(y) = \frac{\mu_L a}{2\mu_L} y^2 + Ay + B \quad (4.3)$$

The no-slip condition  $u = 0$  at the wall ( $y = 0$ ) gives  $B = 0$ . At the liquid film surface ( $y = t$ ), the shear stress is negligible due to the much lower viscosity of the air in the channel, and thus

$$\mu_L \left. \frac{\partial u}{\partial y} \right|_{y=t} = 0 \quad (4.4)$$

giving  $A = -\mu_L a t / \mu_L$ . The resulting velocity profile throughout the liquid film is then

$$u(y) = \frac{\mu_L a}{2\mu_L} y(2t - y) \quad (4.5)$$

This can be integrated across the liquid film to give the volume flow rate per unit circumferential distance,  $q/d$ , as

$$\frac{q}{d} = \int_0^t u(y) dy = \frac{\mu_L a}{3\mu_L} t^3 \quad (4.6)$$

Recalling that  $a = R^{-2}$ , the liquid film thickness is then

$$t = \frac{3}{\mu_L}^{1/3} \frac{\mu_L q}{R^{-2} d}^{1/3} \quad (4.7)$$

in agreement with the result from the simple physical analysis in the previous section. Note that the proportionality constant in the earlier result is essentially unity. From  $u(y)$  in (4.5), the bulk average film velocity  $U_b = q/d$  is also given by (4.6). For the typical slinger in §4.1.5, this gives  $U_b = 7.5$  m/sec, as was used in §4.1.1.

#### 4.1.4. Effect of channel shape

The result in (4.7) gives the limiting film thickness for a slinger with circular channels. This may be readily extended to any other cross-sectional shape, since as noted above the principal effect of the channel shape is to determine the surface area over which the film is spread. Thus for a cross-sectional shape with perimeter  $P$ , the surface area will be the same as for a circular channel having the equivalent diameter

$$d = \frac{P}{\pi} \quad (4.8)$$

The film thickness for channels with noncircular cross sections should therefore be the same as for a circular channel with the same equivalent diameter  $d$ . For example, the limiting film thickness for a slinger with slotted channels, having cross-sectional dimensions  $h$  and  $b$ , is therefore

$$t = \frac{3}{\mu_L}^{1/3} \frac{\mu_L q}{R^{-2} d}^{1/3} \quad (4.9)$$

where

$$d = \frac{2}{\pi} (h + b) \quad (4.10)$$

is the equivalent diameter giving the same circumference as the slot.

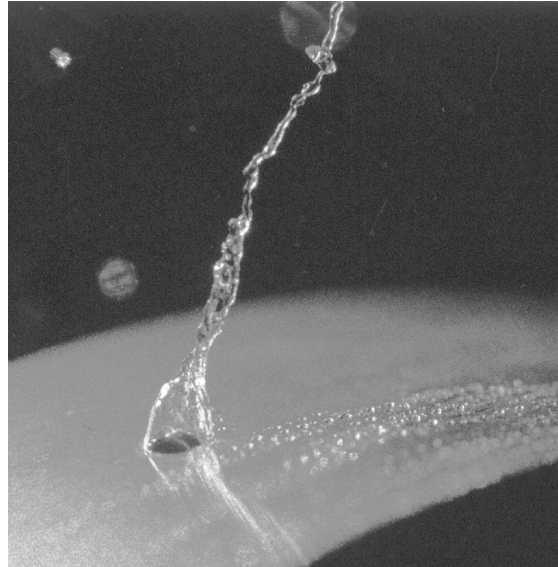
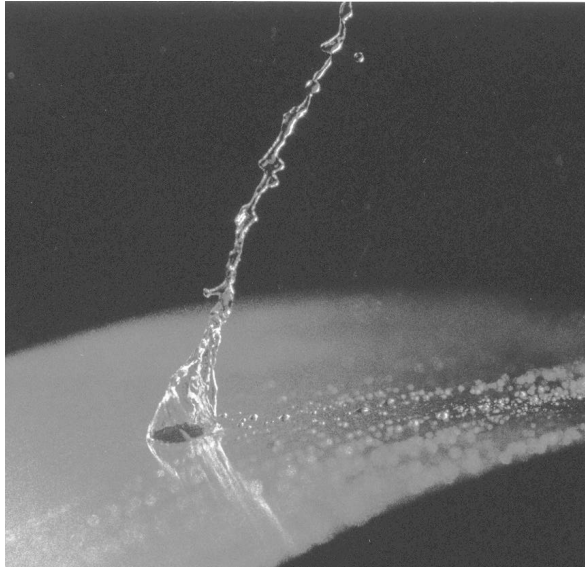


**Fig. 7.** Two typical instantaneous oblique views of subcritical liquid breakup in the large round hole (LR) slinger in Table 1, at a comparatively low rotation rate. At these low  $We$  conditions, the liquid film that issues from the periphery of the hole is drawn together by surface tension into a single large-diameter ligament, which then undergoes classical Rayleigh breakup.

#### 4.1.5. Practical film thicknesses and implications

The results in (4.7) or (4.9) can be used to determine the film thickness for a notional slinger that corresponds roughly to the geometry and operating conditions typical of real fuel slingers. Taking the slinger diameter as 4-in. ( $R = 5$  cm) with  $N = 32$  circular holes each having 0.030-in. diameter ( $d = 0.8$  mm), the rotation rate as 30,000 rpm ( $\omega = 3100$  rad/sec), and total fuel mass flow rate  $M = 50$  lb/hr, with liquid viscosity  $\mu_L$  and density  $\rho_L$  corresponding to Jet-A fuel at 10 °C ( $\mu_L/\rho_L = 2 \cdot 10^{-6}$  m<sup>2</sup>/sec), then gives the limiting film thickness as

$$t = 10 \mu\text{m} = 0.0004\text{-in.}$$

This result is remarkable for several reasons. First, it is exceedingly small in comparison with the 800  $\mu\text{m}$  channel diameter. Thus the relative film thickness  $s = (t/d) = 0.01$ , confirming that the channel serves mainly to provide surface area over which the liquid film is spread. This indicates that the channel shape itself is essentially irrelevant to the film thickness; only the perimeter of its cross section matters, essentially justifying the equivalent diameter concept in §4.1.4.

Moreover, this thickness suggests that surface finish of the channels must be kept significantly smaller than the 0.0004-in. film thickness in order to attain near-uniform film thickness; a poorer surface finish will lead to “film channeling” (see §4.2) that can produce nonuniform film thickness and thus larger drop sizes and larger drop dispersion during the primary film breakup process (see §4.3). This is consistent with practical experience with fuel slingers, which has shown that high surface finish of the channels must be maintained to achieve good atomization properties.

Finally, given the very weak (1/3-power) dependence in (4.7) of the limiting film thickness  $t$  on all other parameters associated with the fuel slinger design and operation, it is unlikely that ei-

ther the small film thickness itself, or the observations noted above that are implied by it, will change dramatically for most practical fuel slingers.

## 4.2 Film Instabilities and Other Nonuniformities

### 4.2.1. Film Reynolds number

The results above assume that the film Reynolds number  $Re_t = Ut/\mu_L$  is sufficiently small for the film flow to remain laminar. Here  $\mu_L/\rho_L$  is the kinematic viscosity of the liquid and  $U$  is the film surface velocity, namely  $u(y=t)$ , which can be obtained from (4.5) as

$$U = \frac{\rho_L R^2 \omega^2}{2\mu_L} t^2. \quad (4.11)$$

For the notional fuel slinger in §4.1.5, the resulting film surface velocity becomes  $U = 11$  m/s, for which the film Reynolds number then becomes  $Re_t = 55$ .

The critical value of  $Re_t$  at which the film becomes inertially unstable can be obtained by noting that the parabolic velocity profile in (4.5) is the same as that in pressure-driven laminar Poiseuille (channel) flow between parallel plates spaced  $2t$  apart. Experiments in such Poiseuille flows show that the instability begins at about  $Re_t = 10^3$ , suggesting that instability may occur in the liquid film at comparable Reynolds numbers. A potentially important difference between the two flows is that the symmetry requirement at the centerline of the Poiseuille flow does not exist at the free surface of the film flow. This can be expected to reduce the maximum  $Re_t$  value at which the film flow remains inertially stable; there is some indirect evidence that the resulting critical value of  $Re_t$  may be around 400. Based on the film Reynolds number obtained in §4.1.5 for a “typical” fuel slinger, it is anticipated that in practical slingers sized for use in small gas turbine engines the resulting film flow will remain below this

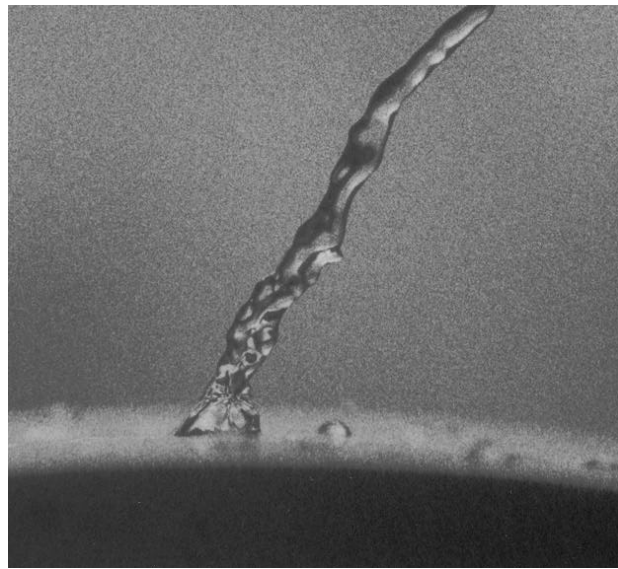
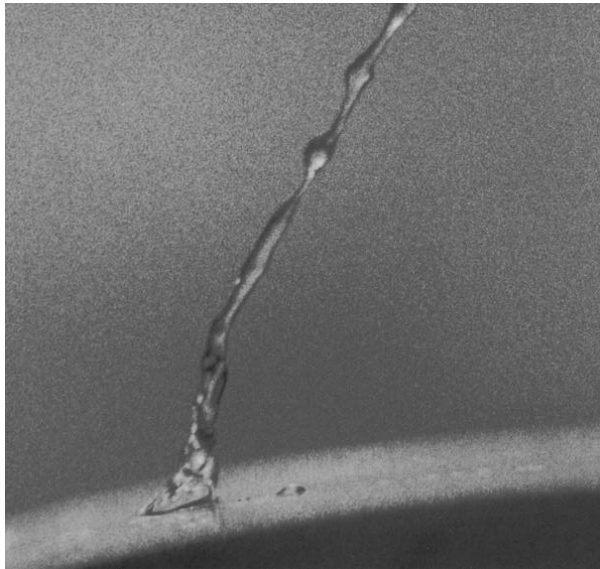


**Fig. 8.** Two typical instantaneous side views of subcritical liquid breakup in the large round hole (LR) slinger at relatively low rotation rate. These side views confirm that the thin liquid film issues from the entire periphery of the hole, indicating that Coriolis effects are insufficient at these conditions to accumulate liquid on the side of the hole opposing the direction of rotation.

critical Reynolds number, and that the results in §4.1 will therefore be applicable.

The film Reynolds number  $Re_f$  is relevant to more than just the applicability of the laminar film flow results obtained in §4.1; it also determines whether the primary breakup of the liquid film past the channel exit will occur in the laminar or turbulent regime. The physical mechanisms responsible for primary film breakup are very different in these two regimes, as noted in §4.3.1. The results above suggest that the liquid fuel films in practical fuel slingers undergo nonturbulent primary breakup.

#### 4.2.2. Film Weber number

Section 4.2.1 addresses “inertial instability” resulting from competition between the steepening of velocity gradients by inertia and the smoothing by viscous diffusion. However in thin-film flows there is another competition, between surface tension and inertia, that can lead to a different type of instability. The parameter that determines the relative importance of surface tension is the inverse of the film Weber number  $1/We_f$ , where  $We_f = \rho_L t U^2 / \sigma_L$  and  $\sigma_L$  is the liquid surface tension. When  $We_f$  is large then the effects of surface tension are small and surface tension instability will not occur. However, if  $We_f$  becomes small enough, then the film can become unstable due to the effect of surface tension. In that case, the nominally uniform film thickness may no longer apply, and the film can instead be drawn by surface tension into streaks that have characteristic dimensions much larger than the nominally uniform film thickness.

For the notional slinger in §4.1.5, with liquid surface tension corresponding to Jet-A fuel at 10 °C ( $\sigma_L = 2 \cdot 10^{-2}$  N/m), the resulting film Weber number is  $We_f = 60$ , which is small enough that surface tension effects might be anticipated. The reduced surface tension at higher temperatures will increase  $We_f$

and could thereby dramatically alter the atomization performance, as indicated by the visualization experiments.

The most relevant of such surface tension driven instabilities in fuel slingers is the “Marangoni effect”, an evaporation-driven surface tension instability. This occurs in multicomponent volatile mixtures when one component evaporates preferentially over others, and in so doing causes an increase in the surface tension. In effect, a preferential evaporation of light solvents at certain locations in the liquid film causes an enrichment of less volatile constituents in the surface layer of the film. A sinusoidal disturbance of the interface will then produce an increase in the evaporation rate at the peaks, and a reduction at the troughs. If the fluid has the property that such evaporation produces an increase in the surface tension, then the resulting faster rate of increase in the surface tension at the peaks draws more liquid toward the peaks, thereby amplifying the effect. The liquid is thereby drawn in at regular intervals, producing narrow rivulets in which the effective film thickness is far larger than the original uniform film thickness. Because the thin film flow in fuel slinger channels involves a fuel, comprised of an inherently volatile mixture of several different components, the potential for Marangoni instability exists. This would, in general, have a detrimental impact on the atomization performance.

#### 4.2.3. Effect of surface nonuniformities

A different but related issue is the effect of surface nonuniformities on the film properties. Owing to the relatively thin nominal film thickness under realistic slinger operating conditions, as noted above, the effect of surface finish within the channels becomes important in setting the actual film thickness that is achieved. If the nominally flat channel wall is actually characterized by roughness depth  $\delta$ , then if  $\delta$  becomes comparable to the nominal film thickness  $t$  the roughness will modify the actual film thickness. The precise effect of the roughness depends on

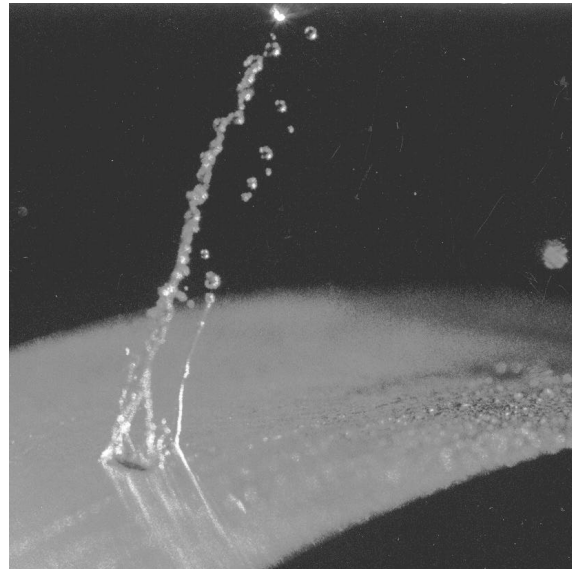
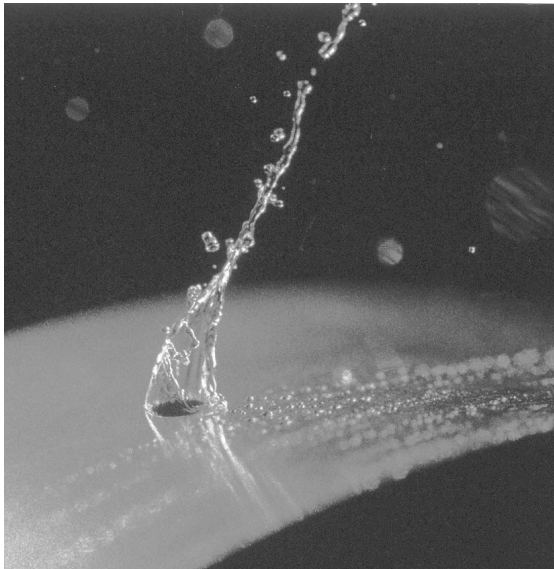


**Fig. 9.** Comparison of subcritical liquid breakup on the large round hole (LR) and short slot hole (SS) slingers in Table 1, confirming that in both cases the liquid film issuing from the hole is drawn into a single ligament that then undergoes Rayleigh breakup. Since the equivalent diameter  $d$  is the same for both holes, the resulting drop sizes are essentially the same despite the different hole geometries.

the relative roughness ( $\epsilon/t$ ). If ( $\epsilon/t$ ) is sufficiently small, then the surface roughness will be irrelevant.

#### 4.2.4. Coriolis-induced nonuniformities

The film thickness in (4.7) and (4.9) assumes that the liquid in the slinger channels experiences only radial (centripetal) acceleration, based on the fact that the Rossby number  $Ro = R/U$  for the film flow is typically about 20 (see §4.1.1). However, while

the lateral Coriolis acceleration is indeed small, it acts on the liquid during the entire time  $T \sim L/U$  that the liquid flows at speed  $U$  along the channel of length  $L$ , and thus it has an integrated effect on the otherwise uniform film thickness. The upper (inviscid) limit on the resulting characteristic lateral displacement of the fluid due to the Coriolis acceleration  $U$  acting over the time  $T$  is then

$$\frac{1}{2} U T^2, \quad (4.12)$$

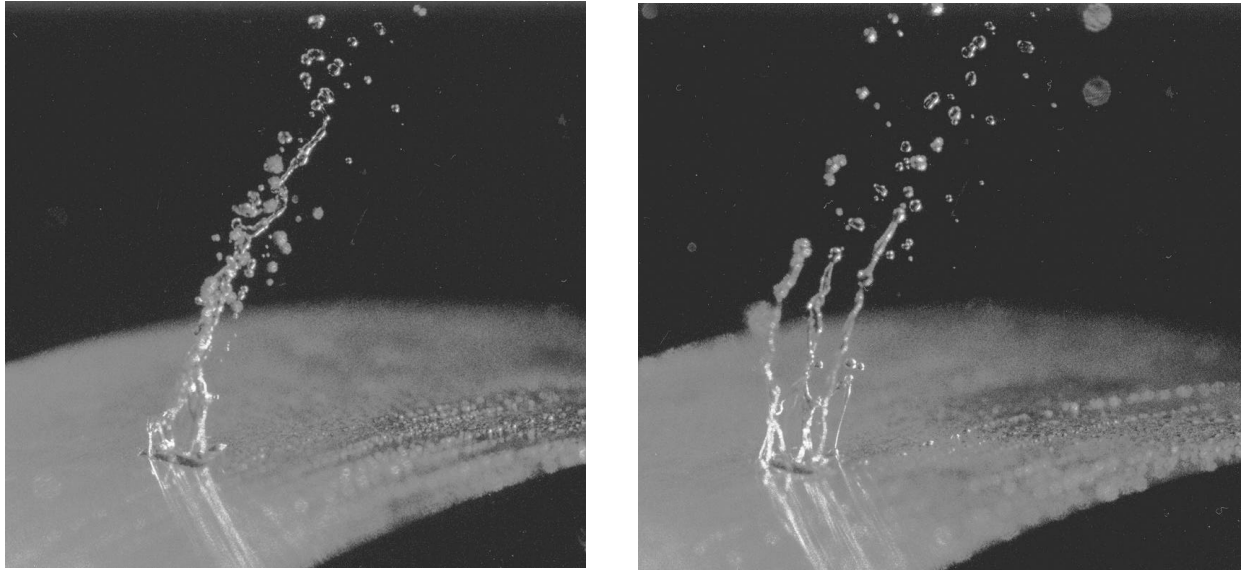


**Fig. 10.** Comparison of subcritical (*a*) and supercritical (*b*) liquid breakup on the short slot hole (SS) slinger. In subcritical breakup, surface tension is sufficiently strong relative to the film inertia to draw the liquid into a single large ligament; in supercritical breakup inertial effects cause the film to break into many smaller ligaments. The transition between these regimes occurs when the inertial time in (2.3) becomes sufficiently large relative to the time scale film collapse in (2.2).

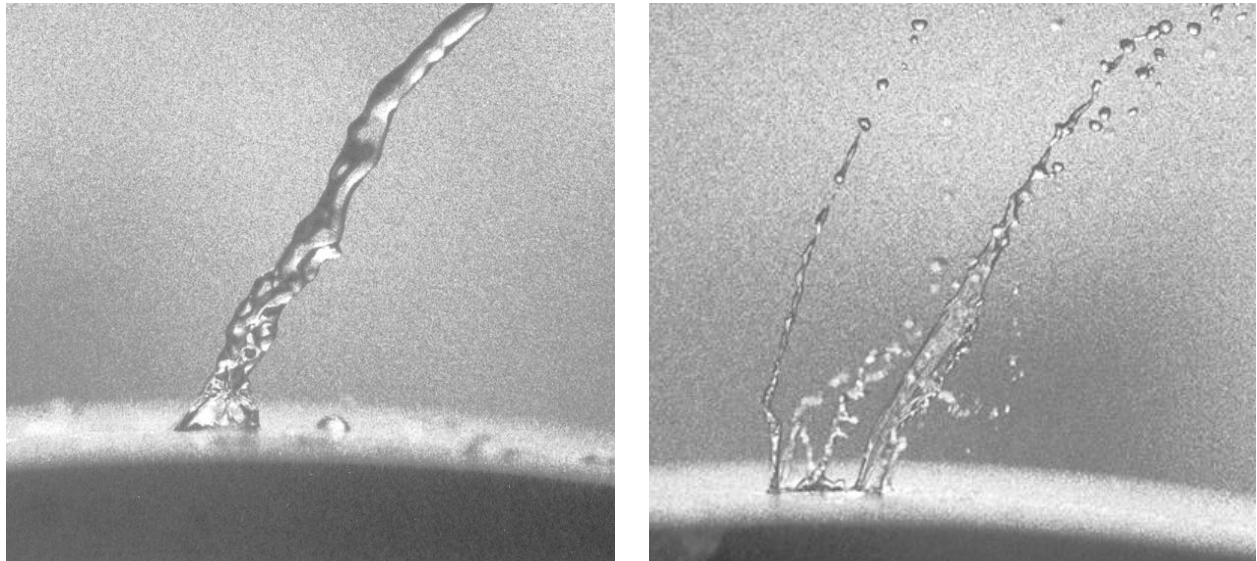


**Fig. 11.** Comparison of subcritical (*a*) and supercritical (*b*) liquid breakup on the square hole (SQ) slinger. The former produces a single large ligament while the latter forms multiple smaller ligaments. The high surface tension near the four corners of the square hole acts to accumulate the liquid from the film into the corners.

and thus the maximum lateral displacement relative to the channel diameter  $d$  is

$$\frac{\Delta}{d} = \frac{1}{2} \frac{L}{d} \frac{L}{R} Ro \quad (4.13)$$

The dependence in (4.13) on the length-to-diameter ratio ( $L/d$ ) of the channels, and on the ratio of channel length to slinger radius ( $L/R$ ), is as would be expected. However, since Coriolis effects become less important as the Rossby number increases, the  $Ro$  dependence is precisely the opposite of what might be expected. This paradox in slingers occurs because both the cen-

trifugal acceleration  $R \omega^2$  and the Coriolis acceleration  $U \omega$  depend on the rotation rate  $\omega$ , and both the residence time  $T$  and the Coriolis force depend on  $U$ . Thus, while  $Ro \gg 1$  correctly indicates that Coriolis forces are much smaller than centrifugal forces, the combined effect with the residence time  $T$  leads to an increase in the relative lateral displacement ( $\Delta/d$ ) with  $Ro$ .

For the typical slinger having  $Ro = 20$ , with channel diameter  $d = 1$  mm, channel length (rim thickness)  $L = 0.25$  in., and radius  $R = 5$  cm, the resulting relative lateral displacement ( $\Delta/d$ )  $\gg 1$ . In

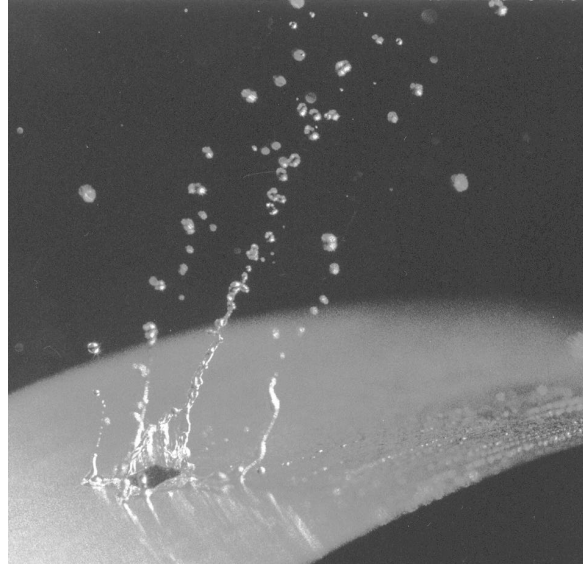
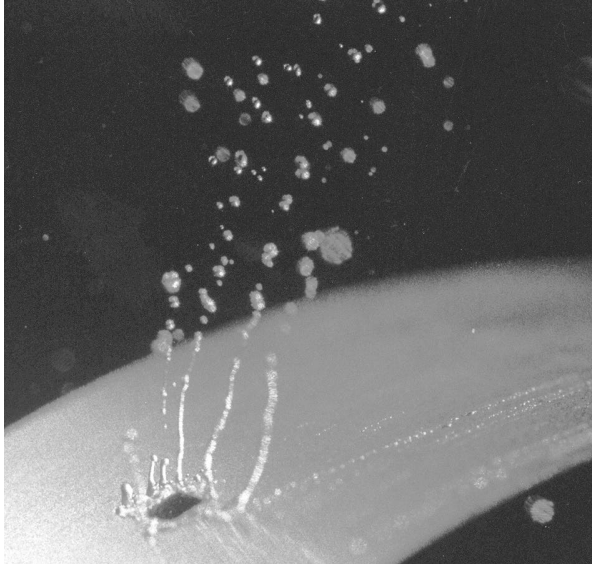


**Fig. 12.** Two typical examples of irregular ligament formation on the square hole (SQ) slinger at 4300 rpm. At these conditions the thin liquid film issuing from the periphery of the hole flows along the slinger face away from the hole rather than separating at the hole edge. The liquid pools on the slinger face until inertia causes it to break into irregular ligaments.

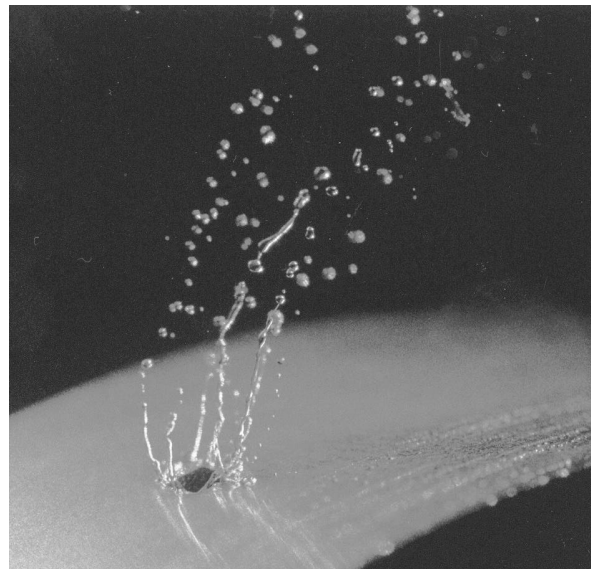
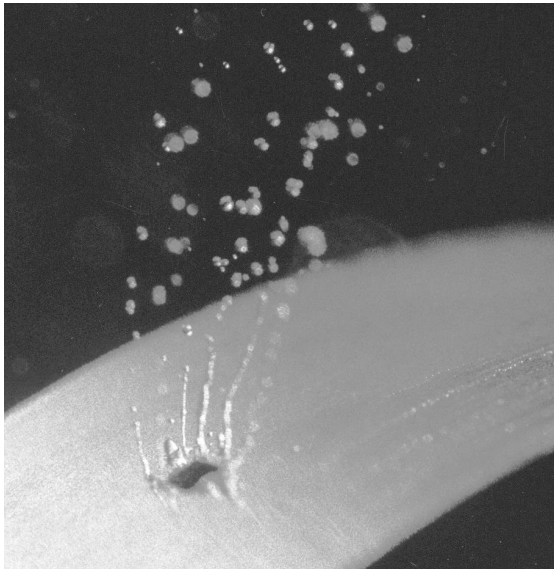


**Fig. 13.** Two examples of ligament formation on the square hole (SQ) slinger at 7800 rpm. At these conditions the liquid film still flows along the slinger face away from the hole, but the higher inertial forces cause it to break into ligaments much closer to the hole. Close inspection reveals liquid flow on the slinger face, and indications of preferential accumulation of liquid near the four corners of the square hole.

other words, under these conditions the integrated effect of the Coriolis acceleration is sufficient to accumulate essentially all of the liquid on the side of the channel that opposes the direction of rotation. The liquid will then exit the channel in a stream having characteristic dimension comparable to the channel diameter  $d$ , rather than in a uniform film having characteristic thickness  $t$ . The liquid breakup process at the channel exit can then be expected to produce drop sizes that scale with the channel diameter  $d$  rather than with the film thickness  $t$ . Moreover, the equivalent diameter concept, which depends on the liquid issuing from the

channels in a thin film, would then also no longer be valid.

On the other hand, if  $(\omega L/d)$  is kept small enough by making the slinger rim thickness  $L$  sufficiently small or the channel diameter  $d$  sufficiently large, then (4.13) shows that the liquid will exit from the channel as a thin film. In that case, the drops that result from the film breakup process can be expected to have diameters comparable to the nominal film thickness  $t$ . Since  $t \ll d$ , a slinger designed to operate in this mode should produce much finer atomization quality.

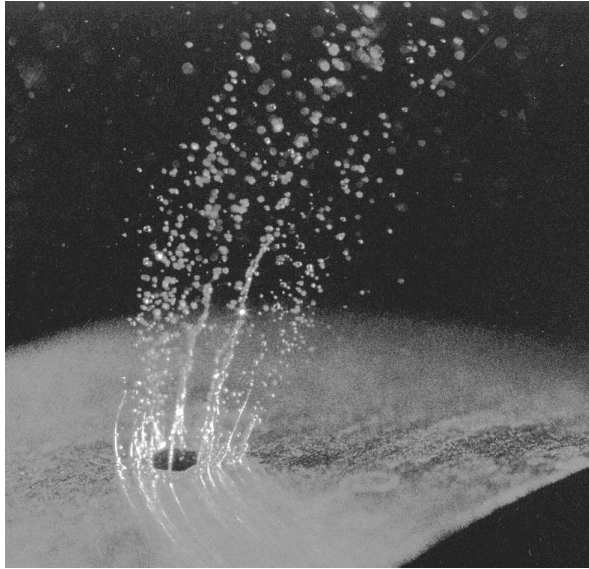


**Fig. 14.** Liquid breakup on the square hole (SQ) slinger at 9500 rpm (a) and at 17,800 rpm (b). As in Figs. 12 and 13, liquid issues from the entire periphery of the hole and flows along the slinger face; this is especially evident at 9500 rpm. At these higher rotation rates, the number of ligaments that form is larger and the ligament diameters are smaller, leading to finer drop sizes.

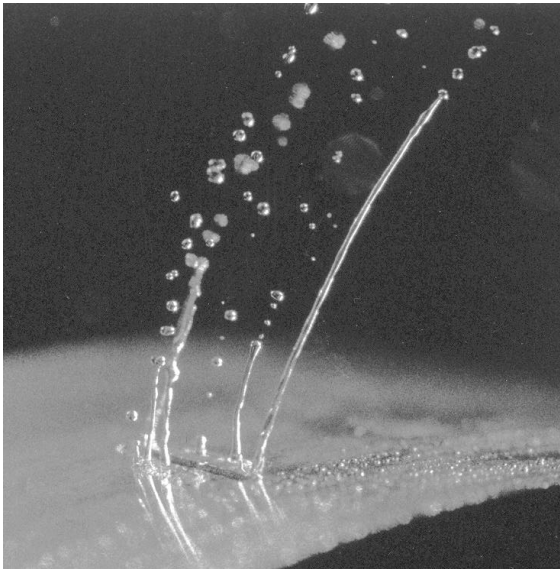


**Fig. 15.** Comparison of liquid breakup on the long slot (LS) slinger at 4300 rpm (a) and at 17,800 rpm (b). At the lower rotation rate, the surface tension at the two ends of the slot draw the liquid film into relatively large ligaments indicative of subcritical breakup. At the higher rotation rate, the liquid undergoes supercritical breakup as the film breaks into many finer ligaments.

The above considerations suggest that, due to the integrated Coriolis effects, “typical” slingers operate in the liquid stream-breakup mode rather than in the liquid film-breakup mode. Indirect experimental evidence of this will be seen in the resulting drop size correlations in §§4 and 5. However, these fundamental considerations also suggest that a reduction of the slinger rim thickness  $L$  or an increase in the channel diameter  $d$  may suffice to allow the slinger to operate in the liquid film-breakup mode, and thereby achieve finer atomization.

### 4.3 Primary Liquid Breakup

This section deals with the breakup of the liquid as it flows from the channel exit and is subjected to the crossflow of air. Basic research has shown that the breakup of a liquid stream by a crossflow occurs by a two-stage process. The first, referred to as “primary breakup”, involves the initial fragmentation of the liquid stream into smaller structures. The second, termed “secondary breakup”, refers to the subsequent fragmentation of these smaller structures by the aerodynamic forces acting on them into a distribution of even smaller drop sizes. This section reviews primary breakup of the liquids; §4.4 deals with the secondary breakup process in fuel slingers.

#### 4.3.1. Turbulent vs. nonturbulent primary breakup

Primary liquid breakup occurs by fundamentally different processes depending on whether the liquid flow entering the gas crossflow is laminar or turbulent. In the case of a turbulent liquid flow, the primary breakup is principally the result of turbulent eddy motions within the liquid that reach the liquid/gas interface and distort this interface. Such “turbulent primary breakup” processes can be understood in terms of the kinetic energy distribution of turbulent eddies of various sizes, and the surface energy required to introduce a distortion of a given size under the ef-

fect of surface tension at the liquid interface. Turbulent primary breakup occurs when the Reynolds number associated with the liquid flow is sufficiently large. However, as noted in §4.2.1, the value of  $Re_l$  resulting from the film flow in a typical slinger channel is too low to produce turbulent motions within the liquid. As a result, turbulent primary breakup is not the mechanism by which the liquid in fuel slingers initially breaks up.

#### 4.3.2. Nonturbulent primary breakup regimes

When  $Re_l$  is sufficiently low, as appears to be the case for slingers, then the resulting “nonturbulent primary breakup” process occurs by a completely different physical mechanism. In this case, aerodynamic forces induced on the liquid by the pressure and viscous stress distribution at the liquid-gas interface lead to deformation and subsequent breakup of the liquid. Depending on the relative importance of inertia, viscosity, and surface tension (*i.e.*, depending on the values of  $We$  and  $Oh$ ), the resulting deformations and breakup take on different forms.

From experimental observations of nonturbulent primary breakup over a wide range of conditions, several distinctly different forms have been noted. Examples of each are shown in Mazallon *et al* (1999). The major forms of breakup are termed “liquid column breakup”, “bag breakup”, “bag-shear breakup”, and “shear breakup”. Each of these applies over a certain regime in the  $We$ - $Oh$  map given by Mazallon *et al* (1999). The applicability of this nonturbulent primary breakup map to fuel slinger atomization rests on the universality of  $We$ ,  $Oh$ ,  $r$ , and  $m$  for characterizing liquid breakup processes (see §2), and on identification of the proper length scale ( $t$  or  $d$ ) relevant to the primary breakup of the liquid as it exits the slinger channels (see §4.2.4).

At low  $Oh$ , for which the boundaries between these various regimes become independent of  $Oh$ , each of these regimes is

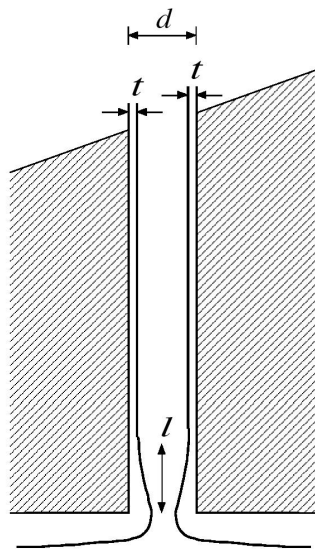


**Fig. 16.** Liquid film flow within a typical slinger channel of diameter  $d$ . The total volume flow rate per channel is  $q$ . After an initial length  $l$ , the film reaches a limiting thickness  $t$  that is key to the film breakup process past the channel exit.

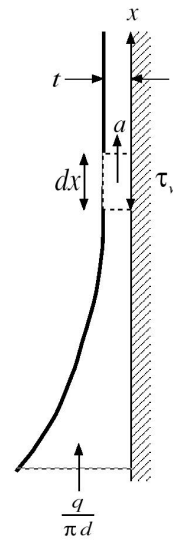


**Fig. 17.** Liquid film flow and thinning along channel wall. The control volume shown corresponds to simple physical analysis for the limiting film thickness  $t \sim (\mu L q / L a d)^{1/3}$ .

found to apply over the following ranges:

$We < 5$	Liquid column breakup
$5 < We < 60$	Bag breakup
$60 < We < 100$	Bag/shear breakup
$We > 100$	Shear breakup

#### 4.3.3. Practical $We$ and $Oh$ values for fuel slingers

For the “typical” fuel slinger noted in §§4.1 and 4.2, with  $R = 5$  cm and  $\Omega = 3000$  rad/sec, the corresponding crossflow velocity  $U_c = R\Omega = 150$  m/sec. With the liquid properties noted earlier for Jet-A fuel, this gives the Weber number based on the nominally uniform film thickness  $t$  as

$$We_t = \frac{\rho_L U_c t}{\sigma} = 0.075, \quad (4.14 a)$$

and the Weber number based on the diameter  $d$  as

$$We_d = \frac{\rho_L U_c d}{\sigma} = 7.5. \quad (4.14 b)$$

It is, at present, unclear whether the more relevant characterization of inertia forces to surface tension forces in the primary breakup process should be based on  $t$  or  $d$ ; there are compelling physical arguments in favor of both (see §4.2.4). It appears likely that the appropriate length scale depends on whether the slinger operates in the supercritical liquid breakup mode ( $t$ ) or in the subcritical liquid breakup mode ( $d$ ). However, it is safe to say that  $t$  and  $d$  should provide lower and upper bounds, respectively, for the range of plausible length scales in the Weber number, and that the appropriate Weber number will fall between the two values given above.

The corresponding Ohnesorge number based on the film thickness  $t$  for the “typical slinger” is

$$Oh_t = \frac{\mu_L}{\rho_L U_c t} = 0.14, \quad (4.15 a)$$

and the Ohnesorge number based on the channel diameter  $d$  is

$$Oh_d = \frac{\mu_L}{\rho_L U_c d} = 0.014. \quad (4.15 b)$$

Again, it is currently unclear whether the characteristic viscous-to-surface-tension ratio expressed by the Ohnesorge number in the primary breakup process should be based on  $t$  or  $d$  (see 4.2.4). However, the appropriate length scale will again be bounded by  $t$  and  $d$ , and thus the appropriate  $Oh$  will fall between the two values given above.

Note, however, that based on available data of Mazallon *et al* (1999) for nonturbulent primary breakup of round liquid jets, both forms of  $Oh$  above suggest that fuel slingers typically operate in the regime of asymptotically small  $Oh$  values for which the breakup process is essentially independent of  $Oh$ , namely at  $Oh < 0.1$ .

While this needs to be confirmed by experiments, it appears to be supported by currently available data, and provides considerable simplification in understanding the atomization performance of fuel slingers (see §5).

The two bounding values for the Weber number given above, however, correspond to different breakup regimes in the  $We$ - $Oh$  map of Mazallon *et al* (1999). The value  $We_t = 0.075$  based on the nominal film thickness  $t$  would indicate liquid column breakup, while the value of  $We_d = 7.5$  based on equivalent diameter  $d$  indicates breakup near the transition between the liquid column mode and the bag mode.

Even more importantly, the dominance of aerodynamic effects in the primary breakup process indicates that the shape and orientation of the liquid relative to the crossflow will play an important role in the breakup. Thus, while the  $We$ - $Oh$  map of Mazallon *et al* (1999) for round liquid jets provides useful qualitative insights into the breakup of the liquid issuing from the slinger channel exit, it is likely to be of only semi-quantitative value. Their results also show the effect of liquid-gas density ratio on the Weber number at which transition occurs from liquid column breakup mode to bag breakup mode. For values of  $r$  anticipated for fuel slinger operation, the effect of density ratio is seen to be comparatively small.

#### 4.4 Secondary Breakup of Drops

This section deals with the secondary breakup of liquid drops formed from the primary breakup process described in §4.3. Secondary breakup of drops occurs by aerodynamic forces exerted on the drop in a manner somewhat similar to that noted in §4.3 for nonturbulent primary breakup. The resulting secondary drop deformations and breakup also take on different forms depending on the relative importance of inertia, viscosity, and surface tension (*i.e.*, depending on the values of  $We$  and  $Oh$ , in this case based on drop diameter).

Four different, more or less distinct, modes of secondary drop breakup have been identified from experimental observations. These are termed “oscillatory deformation” (*i.e.*, no breakup), “bag breakup”, “multimode breakup”, and “shear breakup”. The multimode regime has, in turn, sometimes been separated into a “bag/plume breakup” mode and a “plume/shear breakup” mode. Each of these applies over a certain regime in the  $We$ - $Oh$  map, as shown by Faeth *et al* (1995). Note that, in such secondary breakup processes for round liquid drops, the relevant length scale in both the Weber and Ohnesorge numbers is the initial drop diameter  $d_0$ , and the relevant velocity scale is the relative velocity between the liquid drop and the gas crossflow.

Examples of each mode are shown by Dai & Faeth (2000). While their visualizations were obtained for individual drops subjected to impulsive shock wave disturbances, their applicability to secondary drop breakup in fuel slinger atomization performance rests on the universality of  $We$  and  $Oh$  based on drop diameter for characterizing secondary liquid breakup processes.

The fact that the secondary drop breakup boundaries in Faeth *et al* (1995) are at least qualitatively similar to the primary liquid breakup boundaries in Mazallon *et al* (1999) is not surprising. In effect, this serves to confirm that the relative importance of inertia, viscous, and surface tension forces in liquid breakup processes are largely independent of the liquid geometry when  $We$  and  $Oh$  are properly defined in terms of the length scale characterizing the liquid geometry.



## 5. Resulting Slinger Performance Correlations

The fundamental considerations in §§2-4 provide the basis for a proper formulation of the atomization performance of fuel slingers in terms of fuel properties, slinger design parameters, and slinger operating parameters. In this section, the results from previous sections are used to develop simple design rules and performance correlations for fuel slingers. These design rules are meant only to apply to round hole slingers; their extension to arbitrary hole geometries requires addressing phenomena of the type noted in §3.

### 5.1 Simplifications Applicable to Fuel Slingers

- It was shown in §2 that any properly normalized measure of the performance should be a function only of the Weber number  $We$ , the Ohnesorge number  $Oh$ , the liquid-gas density ratio  $r$ , the liquid-gas viscosity ratio  $m$ , and the relative film thickness  $s$ .
- It was shown in §§4.3 and 4.4 that, at the comparatively low values of  $Oh$  relevant to practical fuel slingers for small gas turbines, the primary and secondary breakup processes become essentially independent of  $Oh$ .
- It was shown in §4.3.2 that, at liquid-gas density ratios  $r$  applicable to the full range of gas turbine operating conditions, the breakup process appears to be largely independent of  $r$  as well.
- Owing to the  $Oh$ -independence at these relatively low values of  $Oh$ , together with the fact that  $Oh$  characterizes the relative importance of viscous effects to surface tension effects, it appears further reasonable to expect that viscous effects are largely negligible, and that therefore the breakup process will be largely independent of the liquid-to-gas viscosity ratio  $m$  as well.
- It was shown in §4 that, for liquid properties and slinger operating conditions applicable to small gas turbines, the nominal film thickness  $t$  is exceedingly small in comparison with the equivalent channel diameter  $d$ , suggesting that typical values of the relative film thickness  $s$  may also be in an asymptotic limit where the effect of  $s$  is negligible.
- It was shown in §4.1 that the nominal film thickness  $t$  changes only weakly with liquid properties and with slinger design and operating parameters, suggesting that the relatively small variations in the length scale ratio  $s$  with fuel properties, design parameters, and operating parameters for actual slingers may have little practical effect on the performance.
- The principal remaining uncertainty is whether the primary and secondary breakup processes are influenced more by the nominal film thickness  $t$  or by the channel diameter  $d$ , however consideration of integrated Coriolis effects in §4.2.4 suggests that the atomization performance of “typical” fuel slingers will scale with  $d$ .

Collectively, these observations provide simplification of the general formulation noted in §2. In the following section, these are used to develop the presumably universal correlation for atomization performance of fuel slingers when operating in this

range of  $We$ ,  $Oh$ ,  $r$ ,  $s$ , and  $m$ .

### 5.2 Nondimensional Drop Size Correlation with $We$

The observations above suggest that the drop size distribution (characterized, for example, by the Sauter mean diameter SMD), when normalized by the appropriate length scale relevant to the breakup process (*i.e.*, the nominal film thickness  $t$  or the channel diameter  $d$ ), will be a function only of the corresponding Weber number  $We$ . Thus for a given hole shape, depending on whether  $t$  or  $d$  is the more relevant length scale, we would expect

$$\frac{SMD}{t} = f(We_t) \quad (5.1a)$$

or

$$\frac{SMD}{d} = f(We_d) \quad (5.1b)$$

where the Weber numbers are defined in (4.14 *a,b*). The former should apply for conditions when the film thickness remains relatively uniform under the effects of surface tension and Coriolis forces. The latter scaling should apply when these effects are sufficiently strong to draw all of the liquid film into a single ligament with thickness comparable to the hole diameter  $d$ . The visualization experiments in §3 suggest that both limits can be encountered in practical fuel slingers under a realistic range of operating conditions.

The functional dependencies on Weber number in (5.1 *a,b*) cannot be determined from analysis alone. However, with the slinger breakup process having been formulated here in terms of the relevant proper dimensionless parameters, it is possible to draw on data from carefully conducted experiments and recast those results in these parameters to determine this dependence.

There have been only very few experimental data reported in the open literature of the atomization performance of fuel slingers. Of these, the experiments of Morishita (1981) from Toyota Motor Co. on small gas turbine slingers appear to be the most carefully done, and cover the widest range of design and operating parameters. Those experiments, which used water as the liquid and considered two fundamentally different slinger designs, obtained data for SMD drop sizes for different combinations of slinger diameters, number of holes, hole sizes, liquid flow rates, and slinger rotation rates. The data will be used here to evaluate the two proposed correlations in (5.1 *a,b*) and to determine the resulting functional dependence on  $We$ .

Using these data, Figs. 18*a,b* compare the correlation achieved by each of (5.1 *a,b*). Significantly better correlation is found with the channel diameter  $d$ , as suggested in §4.2.4 based on the relative lateral displacement in (4.13). This indicates that, due to Coriolis effects, the liquid exits from the slinger channels as a stream with characteristic dimension more comparable to the diameter  $d$  than to the nominal film thickness  $t$ .

Furthermore, the straight-line correlation evident in Fig. 18*b* reflects a power-law form of the functional dependence on  $We_d$  where the exponent is obtained from the slope of the line. Note that, since this correlation is obtained from an analysis in terms of the proper fundamental scaling variables, the proportionality constant should be a truly universal constant, applicable to all fuel properties, all slinger geometries with round holes, and all

operating parameters for which the observations noted above apply. For slingers with noncircular holes, the constant will be different but the scaling should otherwise be identical.

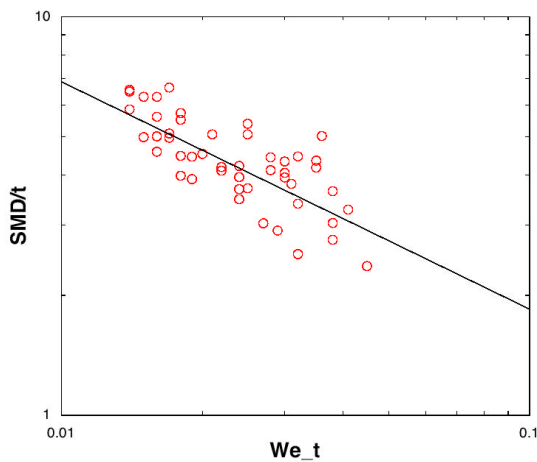
Using the exponent and proportionality constant obtained from Fig. 18b, the correlation between predicted and measured SMD values is shown in Fig. 19. It is evident that, over the entire range of conditions represented in these data, good agreement with measured drop sizes is obtained.

### 5.3 Tests for Further $Oh$ and $s$ Effects

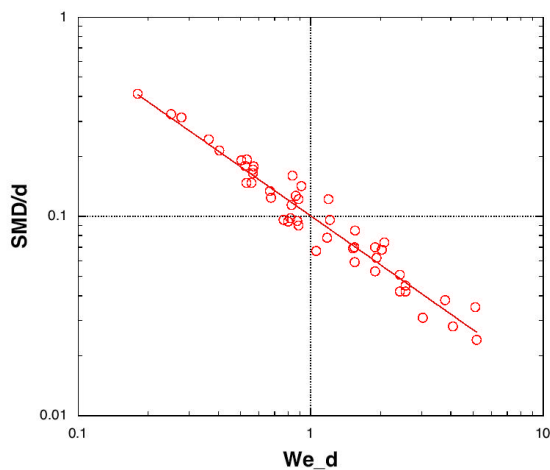
Deviations from the solid lines in Figs. 18a,b and Figs. 19a,b are due in part to scatter in the data that results from the relatively simple method used in the experiments to measure drop sizes, but may also reflect weak effects of the Ohnesorge number  $Oh$ ,

the relative film thickness  $s$ , the density ratio  $r$ , or the viscosity ratio  $m$ . The Toyota data do not permit any assessment of  $r$  or  $m$  effects, since all of the data involve the same values for these parameters. However, they do permit an assessment of any  $Oh$  or  $s$  effects, since these vary considerably among the data points.

Accordingly, Figs. 20a,b show the correlation with  $Oh$  of the ratio of predicted-to-measured SMD values, where the predicted values come from (5.1). Thus any correlation that appears in these results would indicate a multiplicative functional dependence on  $Oh$  in (5.1). It is evident in Fig. 20a that there is no significant correlation with  $Oh$  based on the nominal film thickness; this is consistent with the conclusions above that these slinger designs involve significant Coriolis effects that force the liquid to exit the channels in streams rather than in thin films,

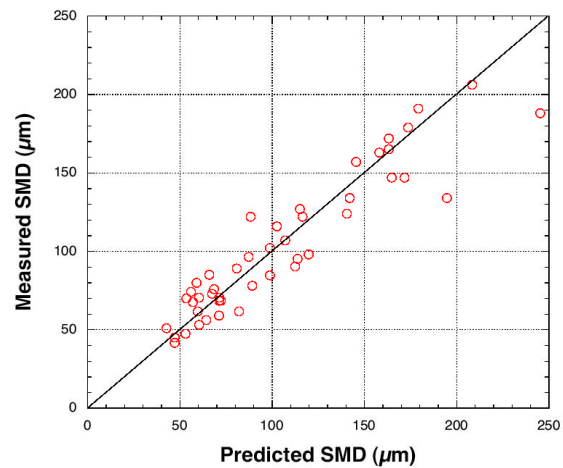


(a) Poorer correlation of SMD with liquid film thickness  $t$  in (5.1a).

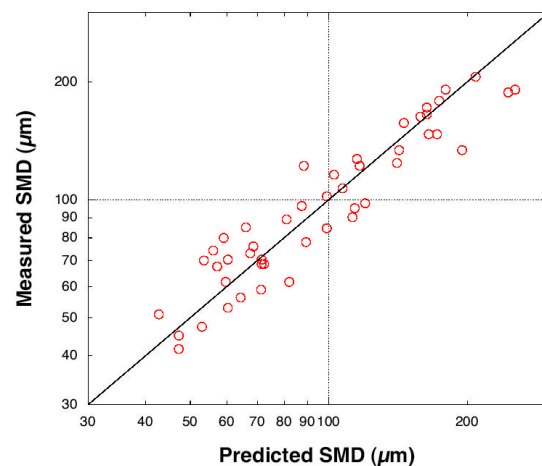


(b) Better correlation of SMD with channel diameter  $d$  in (5.1b).

**Fig. 18.** Comparison of correlations in (5.1a,b) to identify which length scale is more directly relevant to the primary and secondary liquid breakup processes in fuel slingers. Significantly higher correlation is obtained by scaling with the channel diameter  $d$  in (5.1b) than with nominal film thickness  $t$  in (5.1a). Raw data are from Morishita (1981).



(a) Linear axes.

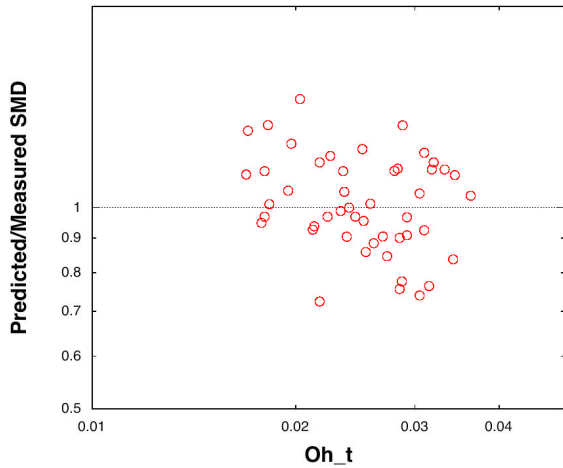


(b) Logarithmic axis.

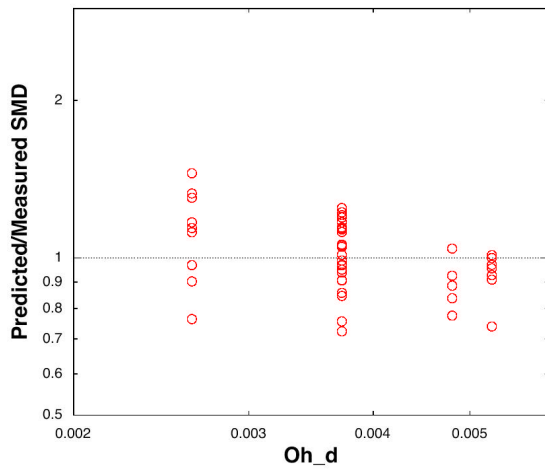
**Fig. 19.** Comparison between predicted and measured atomization performance as characterized by SMD drop size in (5.1b). Measured values are from Morishita (1981).

and serves to further reinforce those conclusions. The results in Fig. 20b suggest a weak power-law correlation with  $Oh$  based on the channel diameter  $d$ , however it is apparent that this correlation is so small in comparison with the remaining scatter in the data as to be of questionable validity. For this reason, no  $Oh$  dependence is proposed in the performance correlation in (5.1).

The evidence at this point is substantial that the slingers in these experiments involve breakup of the liquid in streams issuing from the channels, rather than as thin films. This would suggest little effect of the nominal film thickness  $t$  on the atomization performance, and thus no correlation with the relative film thickness  $s = t/d$ . To test this, Fig. 21 shows the correlation with  $s$



(a) Correlation with  $Oh$  based on film thickness  $t$ .



(b) Correlation with  $Oh$  based on channel diameter  $d$ .

**Fig. 20.** Correlation with Ohnesorge number  $Oh$  of the ratio of predicted-to-measured SMD values. Weak  $Oh$  correlation evident in these results suggests a residual viscosity effect, implying a multiplicative functional dependence on  $Oh$  in (5.1), however the effect seen here is smaller than the scatter in the data. Raw data are from Morishita (1981).

of the ratio of predicted-to-measured SMD values. It is readily apparent that there is no effect of  $s$  on the atomization performance.

## 6. Summary and Conclusions

The results from this study can assist in understanding the performance of existing fuel slingers, in designing improved slingers, and in improving predictions of spray characteristics needed as inputs for CFD modeling of gas turbine combustors. Major conclusions relevant to practical fuel slinger design and operation include:

- Any properly normalized measure of fuel slinger atomization performance is a function only of the Weber and Ohnesorge numbers,  $We$  and  $Oh$ , the liquid-gas density and viscosity ratios  $r$  and  $m$ , and the relative film thickness  $s$ .
- At the comparatively low values of  $Oh$  relevant to practical fuel slingers for small gas turbines, the liquid breakup process becomes essentially independent of  $Oh$ .
- The  $Oh$ -independence indicates that viscous effects are largely negligible, and therefore the breakup process becomes largely independent of the liquid-to-gas viscosity ratio  $m$  as well.
- At liquid-gas density ratios  $r$  applicable to the full range of gas turbine operating conditions, the breakup process is found to be essentially independent of  $r$  as well.
- At  $We$  values relevant to practical fuel slingers, the primary liquid breakup process will occur near the transition between the liquid column mode and the bag mode.

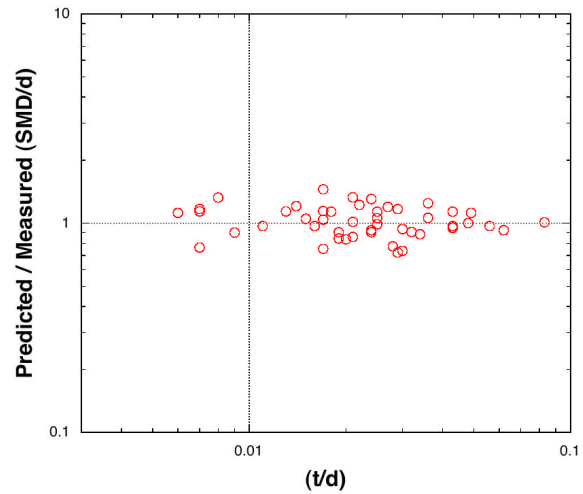


**Fig. 21.** Correlation with relative film thickness  $s = (t/d)$  of the ratio of predicted-to-measured SMD values. A significant correlation would imply that the result in (5.1) should involve a multiplicative functional dependence of the form  $f(t/d)$ . No significant correlation is evident in the data, suggesting that relative film thickness is irrelevant to SMD for “typical” slingers operating in the liquid stream breakup mode. Raw data are from Morishita (1981).

- For liquid properties and slinger operating conditions applicable to small gas turbines, the nominal film thickness  $t$  in the slinger channels is sufficiently small in comparison with the channel diameter  $d$  that the effect of  $s$  also becomes negligible; for typical slingers  $t \approx 10 \mu\text{m}$ .
- For typical slingers the peak film speed is  $U_p \approx 11 \text{ m/s}$  and the average speed is  $U_b \approx 7.5 \text{ m/s}$ , giving a Rossby number of  $Ro \approx 20$  and indicating that the lateral Coriolis force on the film is typically about 5% of the centrifugal force.
- The Reynolds number associated with liquid flow in the channels is sufficiently low that the liquid breakup occurs via the “nonturbulent primary breakup mechanism”.
- These considerations indicate that for a given hole shape the atomization performance of typical slingers is properly given by a fundamental correlation expressed solely in terms of the channel diameter  $d$  and the Weber number  $We_d$ .
- This fundamental prediction provides excellent correlation of experimental data of Morishita (1981) on the atomization performance of small gas turbine slingers for various combinations of slinger diameters, number of holes, hole sizes, liquid flow rates, and slinger rotation rates.
- Constants in this fundamental correlation are obtained by plotting the raw data of Morishita (1981) in the variables indicated by the present fundamental analysis.
- The atomization performance is principally dependent on the peripheral velocity  $U_c = R \omega$  of the slinger, with resulting drop sizes following a power-law scaling in  $U_c$  if all other parameters are kept constant.
- The performance is weakly dependent on the channel diameter  $d$ , with drop sizes following a power-law scaling in  $d$  if all other parameters are kept constant.
- The drop size distribution is independent of the fuel flowrate  $Q$  or the number of slinger channels  $N$ .
- The atomization performance does not depend on the liquid viscosity  $\mu_L$ .

#### Acknowledgements

Discussions on fuel slinger applications in small gas turbines with J. Condevaux and G. Defever of Williams International provided the motivation for the present study. Williams International provided the fuel slingers used in this study. J. Mullinas assisted with the Nd:YAG laser visualization experiments. J. Zimmerman provided assistance in locating data on fuel slinger performance in the open literature. G. Faeth provided an advance copy of one of the papers (Aalburg *et al* 2001) used in this study.

#### References

- Aalburg, C., Faeth, G.M. & van Leer, B. (2001) Properties of nonturbulent round liquid jets in uniform crossflows. Submitted to *Int. J. Multiphase Flow*.
- Bayvel, L. & Orzechowski, Z. (1993) *Liquid atomization*. Taylor & Francis, Washington, D.C.
- Dai, Z. & Faeth, G.M. (2001) Temporal properties of secondary

drop breakup in the multimode breakup regime. *Int. J. Multiphase Flow* **27**, 217-236

Faeth, G.M., Hsiang, L.-P. & Wu, P.-K. (1995) Structure and breakup properties of sprays. *Int. J. Multiphase Flow* **21** (Suppl.), 99-127.

Lefebvre, A.. (1989) *Atomization and sprays*. Taylor & Francis, Washington, D.C.

Lin, S.P. & Reitz, R.D. (1998) Drop and spray formation from a liquid jet. *Annu. Rev. Fluid Mech.* **30**, 85-105.

Mazallon, J., Dai, Z. & Faeth, G.M. (1999) Primary breakup of nonturbulent round liquid jets in gas crossflows. *Atomization and Sprays* **9**, 291-311.

Morishita, T. (1981) A development of the fuel atomizing device utilizing high rotational speed. ASME Paper No. 81-GT-180, American Society of Mechanical Engineers, New York, NY.

Rogo, C. & Trauth, R.L. (1974) Design of high heat release slinger combustor with rapid acceleration requirement. SAE Paper No. 74-0167, Society of Automotive Engineers, New York, NY.

Unverdi, S.O. & Tryggvason, G. (1999) The shear breakup of an immiscible fluid interface. In *Proc. of the C.S. Yih Memorial Symposium* (W. Shyy, Ed.) Cambridge Univ. Press, Cambridge.

Wu, P.K., Ruff, G.A. & Faeth, G.M. (1991) Primary breakup in liquid-gas mixing layers. *Atomization and Sprays* **1**, 421-440.